National Library of Canada
Canadian Theses Service
Ottawa, Canada
K1A 0N4

Bibliothèque nationale du Canada
Services des thèses canadiennes

CANADIAN THESES

THÈSES CANADIENNES

NOTICE

The quality of this microfiche is heavily dependent upon the quality of the original thesis submitted for microfilming. Every effort has been made to ensure the highest quality of reproduction possible.

If pages are missing, contact the university which granted the degree.

Some pages may have indistinct print especially if the original pages were typed with a poor typewriter ribbon or if the university sent us an inferior photocopy.

Previously copyrighted materials (journal articles, published tests, etc.) are not filmed.

Reproduction in full or in part of this film is governed by the Canadian Copyright Act, R.S.C. 1970, c. C-30. Please read the authorization forms which accompany this thesis.

AVIS

La qualité de cette microfiche dépend grandement de la qualité de la thèse soumise au microfilmage. Nous avons tout fait pour assurer une qualité supérieure de reproduction.

S'il manque des pages, veuillez communiquer avec l'université qui a conféré le grade.

La qualité d'impression de certaines pages peut laisser à désirer, surtout si les pages originales ont été dactylographiées à l'aide d'un ruban usé ou si l'université nous a fait parvenir une photocopie de qualité inférieure.

Les documents qui font déjà l'objet d'un droit d'auteur (articles de revue, examens publiés, etc.) ne sont pas microfilmés.

La reproduction, même partielle, de ce microfilm est soumise à la Loi canadienne sur le droit d'auteur, SRC 1970, c. C-30. Veuillez prendre connaissance des formules d'autorisation qui accompagnent cette thèse.

THIS DISSERTATION HAS BEEN MICROFILMED EXACTLY AS RECEIVED

LA THÈSE A ÉTÉ MICROFILMÉE TELLE QUE NOUS L'AVONS REÇUE

NL 339 (r. 86/01)

Canada

109

0-315-26842-5

National Library of Canada | Bibliothèque nationale du Canada

Canadian Theses Division | Division des thèses canadiennes

Ottawa, Canada
K1A 0N4

PERMISSION TO MICROFILM — AUTORISATION DE MICROFILMER

• Please print or type — Écrire en lettres moulées ou dactylographier

Full Name of Author — Nom complet de l'auteur

LORI LYNN SMALL

Date of Birth — Date de naissance

August 11, 1958

Country of Birth — Lieu de naissance

Canada

Permanent Address — Résidence fixe

241 Beverly Hills
53110 - Rge. Rd. 213
Ardrossan, Alberta T0B 0E0

Title of Thesis — Titre de la thèse

Fast, Low Jitter Spark Gap Switching

University — Université

University of Alberta

Degree for which thesis was presented — Grade pour lequel cette thèse fut présentée

Master of Science

Year this degree conferred — Année d'obtention de ce grade

1983

Name of Supervisor — Nom du directeur de thèse

Prof A.A. Offenberger

Permission is hereby granted to the NATIONAL LIBRARY OF CANADA to microfilm this thesis and to lend or sell copies of the film.

The author reserves other publication rights, and neither the thesis nor extensive extracts from it may be printed or otherwise reproduced without the author's written permission.

L'autorisation est, par la présente, accordée à la BIBLIOTHÈQUE NATIONALE DU CANADA de microfilmer cette thèse et de prêter ou de vendre des exemplaires du film.

L'auteur se réserve les autres droits de publication; ni la thèse ni de longs extraits de celle-ci ne doivent être imprimés ou autrement reproduits sans l'autorisation écrite de l'auteur.

Date

Sept 14, 1983

Signature

L. Small

NL-91 (4/77)

THE UNIVERSITY OF ALBERTA

FAST, LOW JITTER SPARK GAP SWITCHING

by

© Lori Lynn Small

A THESIS

SUBMITTED TO THE FACULTY OF GRADUATE STUDIES AND RESEARCH

IN PARTIAL FULFILMENT OF THE REQUIREMENTS FOR THE DEGREE

OF MASTER OF SCIENCE

DEPARTMENT OF ELECTRICAL ENGINEERING

EDMONTON, ALBERTA

Fall, 1983

THE UNIVERSITY OF ALBERTA

RELEASE FORM

NAME OF AUTHOR Lori Lynn Small

TITLE OF THESIS FAST, LOW JITTER SPARK GAP SWITCHING

DEGREE FOR WHICH THESIS WAS PRESENTED MASTER OF SCIENCE

YEAR THIS DEGREE GRANTED Fall, 1983

Permission is hereby granted to THE UNIVERSITY OF ALBERTA LIBRARY to reproduce single copies of this thesis and to lend or sell such copies for private, scholarly or scientific research purposes only.

The author reserves other publication rights, and neither the thesis nor extensive extracts from it may be printed or otherwise reproduced without the author's written permission.

(SIGNED) Lori Small

PERMANENT ADDRESS:

241 Beverly Hills
53110 Bge Rd 213
Ardrossan, Alberta T0B
T0B 0E0

DATED September 16, 1983

THE UNIVERSITY OF ALBERTA

FACULTY OF GRADUATE STUDIES AND RESEARCH

The undersigned certify that they have read, and recommend to the Faculty of Graduate Studies and Research, for acceptance, a thesis entitled FAST, LOW JITTER SPARK GAP SWITCHING submitted by Lori Lynn Small in partial fulfilment of the requirements for the degree of MASTER OF SCIENCE.

...Allan D. Stanbergen.....

Supervisor

.....

.....

Co-Supervisor

Date...August..10,..1983....

TO MY PARENTS

ABSTRACT

This investigation is concerned with the development of a low inductance, low jitter, electrically triggered, high voltage spark gap. The inductance and jitter characteristics of an annular rail spark gap switch are investigated and the results compared with a standard 3-electrode spark gap. Three trigger electrode geometries - blade, dull and sawtooth edge - are tested for the effects of different field stresses on the spark gap switching performance. All possible polarity combinations are applied to the high voltage and trigger electrodes of the rail gap, and the switching behavior is evaluated for each case. Finally, the effect of photo-preionization from bare sparks on the spark gap switching performance is explored.

ACKNOWLEDGEMENTS

The author wishes to express her thanks to Prof. A. A. Offenberger for his guidance and support in this research. Thanks are also extended to Dr. D. C. D. McKen for his inspiration and technical advice. Further acknowledgement goes to the plasma research group, Mr. H. Gans and the machine shop staff at the University of Alberta Department of Electrical Engineering.

Table of Contents

Chapter — Page

1. INTRODUCTION 1

1.1 MOTIVATION FOR THESIS 1

1.2 GENERAL FEATURES OF SPARK GAP DESIGN 4

2. REVIEW OF THE THEORY OF SPARK GAP BREAKDOWN 9

2.1 THE ELECTRON AVALANCHE 10

2.2 THE SPARKING MECHANISM 13

3. EXPERIMENTAL PROCEDURE 17

3.1 OUTLINE OF RESEARCH 17

3.2 DESCRIPTION OF SPARK GAP DESIGN 18

3.3 DESCRIPTION OF CIRCUIT DESIGN 23

3.3.1 CIRCUIT GEOMETRY 23

3.3.2 TRIGGER PULSE CIRCUITRY 27

3.3.3 OPERATING VOLTAGES AND PRESSURES 29

3.3.4 CIRCUITRY FOR PREIONIZATION 30

3.4 MEASUREMENT PROCEDURE AND DIAGNOSTICS 31

4. RESULTS OF THE 3-ELECTRODE SPARK GAP EXPERIMENT 35

4.1 INDUCTANCE AND RESISTANCE OF THE 3-ELECTRODE SPARK GAP 35

4.2 JITTER MEASUREMENTS OF THE 3-ELECTRODE SPARK GAP 37

4.3 CONCLUSIONS OF THE 3-ELECTRODE SPARK GAP EXPERIMENT 37

5. RESULTS OF THE ANNULAR RAIL SPARK GAP EXPERIMENT 38

5.0.1 DEFINITIONS OF ADOPTED NOTATION 38

5.1 DISCUSSION OF OBSERVED WAVEFORMS 39

5.1.1 CALCULATIONS OF DELAY AND JITTER TIMES 46

5.1.2 RAIL SPARK GAP AND EXTERNAL DISCHARGE CIRCUIT INDUCTANCE CALCULATIONS 47

5.2 DISCUSSION OF RESULTS 50
6. CONCLUSIONS 58
REFERENCES 61
VITA 63

LIST OF TABLES

Table		Page
5-1.	Delay, Jitter and Inductance Results of the Annular Rail Gap with a Blade Trigger Electrode.	52
5-2.	Delay, Jitter and Inductance Results of the Annular Rail Gap with a Dull Trigger Electrode.	53
5-3.	Delay, Jitter and Inductance Results of the Annular Rail Gap with a Sawtooth Trigger Electrode.	54

LIST OF FIGURES

Figure		Page
1-1.	The KrF Laser Facility at the University of Alberta.	2
1-2.	Basic Electrode Configurations of Three Common Spark Gaps.	5
3-1.	The 3-electrode Spark Gap Design.	19
3-2.	The Annular Rail Spark Gap Design.	20
3-3.	The Three Trigger Electrodes.	22
3-4.	Circuit Diagram of the 3-electrode Spark Gap Experiment.	24
3-5.	Circuit Diagram of the Rail Spark Gap Experiment.	25
3-6.	The Annular Rail Spark Gap Discharge Circuit Geometry.	26
3-7.	The L-R-C Equivalent Circuit Model of the Discharge Circuitry.	32
4-1.	Current of the 3-electrode Gap Discharge Circuit.	36
5-1.	Observed Trigger Voltage of the Rail Gap Experiment with a Blade Trigger Electrode and +/- Polarity Combination.	41
5-2.	Observed Trigger Voltage of the Rail Gap Experiment with a Blade Trigger Electrode and +/+ Polarity Combination.	41
5-3.	Observed Trigger Voltage of the Rail Gap Experiment with a Sawtooth Trigger Electrode and -/- Polarity Combination.	42
5-4.	Observed Trigger Voltage of the Rail Gap Experiment with a Dull Trigger Electrode and +/+ Polarity Combination.	42
5-5.	The Discharge Current Differential with Respect to Time that was Observed when a +/+p Polarity was Applied to the Rail Gap and Sawtooth Trigger Electrode.	43
5-6.	Characteristic Current Discharge Waveforms when a +/+ Polarity Combination is Applied to the Rail Gap and Blade, Dull and Sawtooth Trigger Electrodes.	46

1. INTRODUCTION

The study of gaseous conduction and its effect on spark gap switch behavior has received a lot of attention from scientists and engineers who work in the area of pulsed power technology. High voltage spark gap switches are employed in particle accelerators, weapons effect simulators, fusion research, and lasers[1]. Recent developments in these areas call for improved spark gap reliability, longer lifetimes, faster energy transfer rates, and lower jitter. The purpose of this thesis is to design and test an electrically triggered spark gap switch that features low inductance and low jitter.

1.1 MOTIVATION FOR THESIS

The following discussion will serve to illustrate by way of practical example some of the demanding requirements on spark gap performance. In this case utilization of spark gaps represent the only practical means of switching the pulsed high voltage and current. Figure 1-1 shows a basic schematic of the KrF laser that is currently under development at the University of Alberta for fusion related research[2]. A nominally 100uJ, 20ns, spectrally narrow pulse is generated in the master oscillator. The first amplifier, A1, serves as an injection locked slave oscillator while the remaining and otherwise identical amplifiers are single pass extracted.

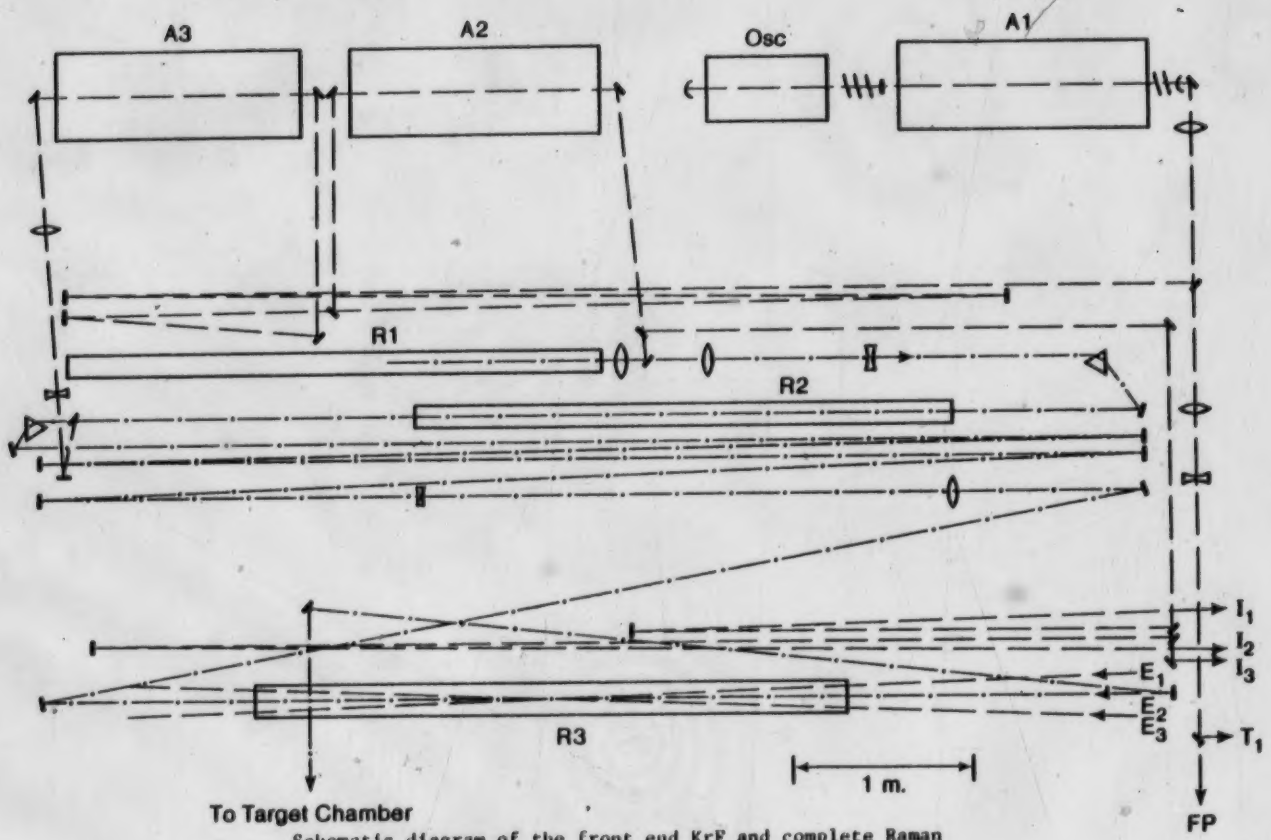

Schematic diagram of the front end KrF and complete Raman compressor system. Legend: A1, A2, A3 - KrF amplifier modules; E_1, E_2, E_3 - Output beams from the E-beam amplifier; FP-Fabry Perot spectral analysis system; I_1, I_2, I_3 - time delayed input beams to extract the E-beam amplifier; Osc-master KrF oscillator; R_1, R_2, R_3 - Methane filled Raman cells; T_1 - KrF pulse to trigger the E-beam amplifier.

Figure 1-1. The KrF Laser Facility at the University of Alberta.(from reference 2)

The utility of the resulting 1.6J of optical energy is three-fold. A portion is used for laser triggering of spark gap switches on an electron-beam pumped KrF power amplifier. Another portion is used to provide a composite 60ns pulse for extraction of the power amplifier and eventual optical compression by beam stacking. The remaining portion is used to generate and tailor a Stokes shifted optical pulse by Raman scattering in methane. The Stokes shifted pulse will be used as a seed for final optical compression by backward Raman amplification[3].

The need for optical compression arises because the lifetime of KrF* is only a few nanoseconds. The laser cannot be operated in the conventional storage mode since the optical energy must be extracted as the electrical energy is deposited. The resulting "uncompressed" optical pulses are too long for application to laser inertial confinement fusion studies where pulse lengths of nominally a few nanoseconds are required.

For efficient and high quality laser performance, switching of the excitation circuits on the various laser modules (involving a total of 13 spark gaps) must be synchronized with a relative jitter of $\leq$1ns standard mean deviation (smd). Furthermore, a test was performed on A3 where part of the excitation circuitry was switched with three parallel spark gaps instead of one. This resulted in a 33% improvement in output energy, dramatically illustrating the importance of low inductance in such an application.

1.2 GENERAL FEATURES OF SPARK GAP DESIGN

Spark gaps are employed in circuits requiring pulsed high voltage and current switching. The basic spark gap switch consists of two electrodes separated by a dielectric that is capable of holding off the applied d.c. electric field, together with some method of triggering the electric breakdown of the dielectric and closure of the spark gap switch. Spark gaps of interest here employ a gaseous dielectric and electrical triggering. There are three common electrode types. These are the trigatron spark gap, the 3-electrode spark gap, and the rail gap. Cross sections showing the electrode configurations of each of these spark gaps are illustrated in figure 1-2. Electrode contours are designed to avoid stress concentration in the dielectric during hold-off and to provide high local stress during triggering. Unfortunately, electrode reshaping by erosion with use degrades the utility of this design parameter. At any rate, application of a high voltage trigger pulse to the trigger electrode produces field distortion and electric stress of sufficient strength to cause dielectric breakdown.

Due to the asymmetry of the distorted electric field, breakdown of the dielectric in one portion of the gap (between the trigger electrode and one of the main spark gap electrodes) will usually occur first. This will be referred to as *the first breakdown stage*. Closure of this portion of the gap will cause the voltage at the trigger electrode to approach that of the main electrode on the side in which the

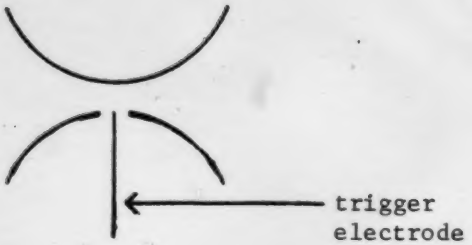

a. The Trigatron Spark Gap

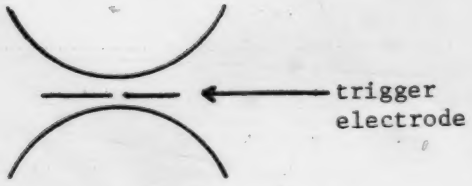

b. The 3-electrode Spark Gap

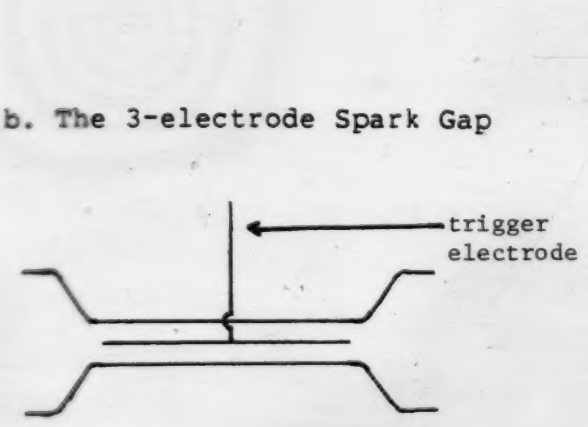

c. The Rail Gap

Figure 1-2.Basic Electrode Configurations of Three Common Spark Gaps.

initial discharge occurred. The intense transient field stress and ionization created by this initial discharge cause sudden closure of the remaining part of the gap.

The simple trigatron spark gap, a single channel closure device, exibits relatively high jitter and inductance. The 3-electrode spark gap is also a single channel closure device, but it has improved jitter characteristics provided the trigger pulse rate-of-rise exceeds 2kV/ns. On the other hand, the rail gap, a multi-channel closure device, has low inductance but relatively high jitter. An additional benefit associated with the multi-channel closure device is reduced electrode erosion due to decreased current density and shot-to-shot random distribution. This not only increases spark gap lifetime but could make electrode contouring a more useful design parameter.

The three basic configurations can be modified to suit certain hold-off voltage and lifetime requirements by changing the gas pressure or type, the electrode material, geometry, and separation. There are many manufactured spark gaps that are available, off the shelf, to the pulsed power engineer. These spark gaps work well if the specifications are not too demanding and if the geometry of the switch is compatible with the designed circuit architecture. Otherwise, custom made designs can be very expensive. This is chiefly due to incomplete understanding of the fundamental mechanisms involved in spark gap closure;

consequently, spark gap design remains an empirical art.

Spark gap jitter is a consequence of two types of delay mechanisms that are associated with breakdown of the dielectric[4]. The first, called the initiatory, or statistical time lag, is the time between the application of the applied breakdown voltage and the arrival of a suitably placed electron that will initiate an avalanche. The second type of delay is the formative time lag which is the period in which the initial avalanche develops into a full, self-sustained discharge. If no method of preionization is applied to the gas, the statistical time lag can be quite large (often by orders of magnitude) and irregular, compared with the formative time lag of the gap.

Under normal conditions the concentration of free electrons in air is 100 to 500 per cubic centimeter[4]. When an overvoltage is first applied to a gap with air as a dielectric, the chance of there being a favourably placed electron is small, so that a waiting period occurs until such an electron appears.

Spark gap jitter is mostly affected by the randomness in the appearance of this free electron, particularly prior to the first breakdown stage. The statistical delay time and jitter can be greatly reduced through some method of preionization which may include doping of the gas[5]. This procedure increases the density of the free electrons in the gap, thereby increasing the probability of occurrence of the electrons that are necessary to initiate breakdown. Laser

and electron-beam preionization techniques have been tested in many configurations with favourable results[6,7]. Furthermore, optical breakdown of the dielectric by focused laser beams provides a low jitter means of triggering. Such techniques are complex and expensive, however, and alternative methods of spark gap triggering must be developed or the existing ones improved for simpler applications. This thesis is concerned with the development and testing of an electrically triggered spark gap which can simultaneously yield low inductance (hence fast voltage and current risetime) and low jitter.

2. REVIEW OF THE THEORY OF SPARK GAP BREAKDOWN

The basic spark gap consists of two electrodes separated by a gaseous dielectric. When a high overvoltage is applied across the electrodes, the dielectric breaks down and delivers a large current to a load. Although this procedure appears to be quite straight forward, the actual mechanisms that lead to dielectric breakdown of a gas are still not well understood. The astronomical range of parameters which describe the particle interactions that occur under transient conditions (typically nanosecond time scales) and inhomogeneous fields are what make this process so difficult to investigate.

Computer simulations are beginning to be of some aid, but the models are either too complicated (or simplified) to provide the user with sufficient accuracy and at the same time reasonable flexibility. E. E. Kunhardt[1] describes the course of breakdown to evolve through three stages.

1. The ionized components of the gas start off as individually charged particles that interact with a background of neutrals.
2. The gas then transforms into a non-ideal plasma (where the Debye length is greater than the plasma dimensions).
3. In the final stage the gas becomes an ideal plasma (that is, the Debye length is less than the plasma dimension).

To this, Kunhardt argues that "No single analytical framework can be used to model this transition."

Further difficulties arise when experimental verification of a particular model is attempted. Diagnostics with subnanosecond resolution have only recently become available. The effect that the external circuit has on the breakdown characteristics can be difficult to decouple from voltage and current measurements. Insufficient light emission during the prebreakdown stage makes the transition very difficult to follow optically. Finally, whatever diagnostic techniques are found to be suitable, unbiased and correct interpretations of the observations are difficult to obtain.

In spite of these difficulties, progress in understanding the mechanisms that lead to gaseous breakdown has been made. A few of the basic phenomena will be described in the following sections. The reader is referred to the bibliography provided at the end of this thesis for a more in-depth study.

2.1 THE ELECTRON AVALANCHE

When an electron moves freely against the direction of an applied field, it will gain energy that is equal to the product of its charge, the magnitude of the field and the distance that it travels. If the field is strong enough that the electron gains sufficient energy to ionize an atom upon collision, the collision will produce a positive[1] ion and another free electron. The two free electrons will gain

---

[1] In intense fields, electrons do not attatch themselves to neutral particles to create negative ions[8].

energy from the electric field and then collide with two more atoms. Once again, if the energy of the collisions is great enough to produce ionization, two more pairs of free electrons and positive ions will be formed. This process, called *field intensified ionization*[8], will continue as long as the external field is applied. Thus, the original current from the free electrons is increased by the additional ionizing collisions that arise from the effect of the applied electric field.

All theories of gaseous conduction are based on this process, which was recognized through experiments conducted by J.S. Townsend[8,9]. Starting with the avalanche model, Townsend developed a theory that could describe the conditions for gaseous breakdown in an electric field.

Townsend found that the current between two electrodes increases exponentially with applied voltage until it reaches a point where it continues to rise, even after the external electric field is removed. The current would continue to rise indefinitely, but it is limited by the constraints of the external circuit. This transition is called a *glow-to-arc transition*, or a *non-self-sustaining to self-sustaining discharge*, and usually occurs with explosive suddenness. The self-breakdown voltage Vs (also called the sparking potential), is defined to be the voltage at which this transition occurs.

Before breakdown, the current from the electron avalanche can be described by the steady-state equation:

$$I=I_{o}\exp(\alpha x) \qquad (2.1)$$

where I_{o} is the current from the initial free electrons and x is the distance travelled by the avalanche. The first Townsend coefficient, α, is the number of ionizing collisions per centimeter of path in the direction of the applied electric field.

The probability of an electron ionizing an atom upon collision depends on its mean free path and the strength of the electric field. The mean free path of an electron varies inversely with the gas pressure. This reasoning and experimental verification has led to the relation[2]

$$\alpha/P=f(E/P) \qquad (2.2)$$

where P is the absolute pressure in Torr and E is the strength of the applied field in volts/cm. The conclusion that α/P is a function of E/P makes the quotient E/P, a measure of the energy gain per mean free path, a very fundamental parameter in the study of gaseous conduction.

---

[2]: Under certain conditions it has been found experimentally that $\alpha/P=A\exp[-B/(E/P)]$, where A and B are constants for a given gas and range of E/P[1,8].

2.2 THE SPARKING MECHANISM

Equation 2.1 describes the process of an electron avalanche, but it does not give any information pertaining to the mechanism of breakdown. It does, however, indicate that other (secondary) processes of ionization must be involved. In order to generate a self-sustained discharge, the initial supply of primary electrons must be replenished, as they move away from the cathode. Two important secondary processes are[1]:

1. positive ion bombardment of the cathode, causing cathode emission of electrons
2. photoionization or photoemission at the cathode from photons that are emitted by collisionally excited atoms.

The effect of these processes and others, can be incorporated into a generalized Townsend coefficient ω, defined to be the number of ions produced per centimeter from general secondary processes. When secondary processes are considered, the current that is produced in an avalanche can be described by the steady state relation[1];

$$I=\frac{I_0\exp(\alpha d)}{1-\omega/\alpha[\exp(\alpha d)-1]} \qquad (2.3)$$

If the distance across the gap d is such that;

$$\omega/\alpha[\exp(\alpha d)-1]=1 \qquad (2.4)$$

the denominator vanishes, marking the transition to a self-sustained discharge.

Equation 2.4 is called *Townsend's breakdown criterion.* The criterion implies that a self-sustained discharge is established only if the conditions of the field, pressure and length of the gap are such that the primary electrons created in the avalanche produce secondary effects sufficient to create new electrons which will sustain the fully developed avalanche[8].

Under transient conditions, the time for a self-sustained avalanche to develop depends on the nature of the secondary processes involved[1]. If ion bombardment of the cathode is the most likely candidate for the secondary process, the formative time of the gap would be limited by the positive ion drift velocity to times of the order of microseconds[1]. Experimental results agree with this limit (and with the Townsend model) for voltages near, or slightly greater ($\leq$120% Vs) than the self-breakdown voltage of the gap[10]. However, if a larger overvoltage is applied to a gap ($\geq$120% Vs), the formative time lag is reduced, indicating that other secondary processes have dominated the sparking mechanism.

The process of electron emission at the cathode by positive ion bombardment is too slow to account for many of the observed speeds of spark formation. Furthermore, at higher pressures, it has been noted that the drift velocity of electrons is also too slow for an avalanche to bridge a gap in the short time lags that have been observed[8].

To account for the short times lags that have been observed at breakdown voltages >120% Vs, other theories based on different sparking mechanisms were developed. The most popular of these theories is the streamer model, proposed by H. Raether. Raether's streamer theory was developed through experiments in a cloud chamber which monitored the progress of an avalanche between two electrodes[11]. Raether proposed that photoionization of the gas (by photons produced through collisions in the avalanche) is the most important secondary process, and that the formative time lag is reduced due to effects of a space charge which develops as the avalanche progresses to the anode.

As the avalanche grows and electrons move towards the anode, a large space charge of positive ions is left behind. The charge distribution inside the avalanche takes the form of a dipole and creates a field that opposes the applied electric field. Although the electric field is reduced inside the avalanche, the electric field at the head of the avalanche is enhanced by the growing electron density.

The basis of the streamer theory is that photons produced by the avalanche ionize the gas ahead, thereby creating a more efficient path for the advancing avalanche, or even initiating secondary avalanches which eventually meet with the main avalanche. Another model, called the two group model has been developed by E.E. Kunhardt and W.W. Byszewski[10]. The two group model is similar to the

streamer model but, instead of photons ionizing the path ahead of the avalanche, Kunhardt and Byszewski propose that the intensified field at the avalanche head produces runaway electrons that are pulled ahead of the main avalanche, thus ionizing the gas in their paths to the anode. Whatever the true spark breakdown mechanism is, for reasons discussed at the beginning of this chapter, the discharge characteristics of a particular spark gap are still basically unpredictable. The research that was conducted for this thesis followed an empirical approach since the primary motivation was to develop a spark gap with improved jitter and inductance characteristics. The procedure of the experimental research is the subject of the next chapter.

3. EXPERIMENTAL PROCEDURE

The purpose of this graduate research was to develop a reliable spark gap with low jitter ($\leq$1ns smd) and low inductance($\leq$10nH). Due to the lack of predictability in spark gap behavior an empirical approach was taken in the spark gap design. The procedure that was followed is summarized below. The subsequent sections in this chapter describe each part of the procedure and apparatus in detail.

3.1 OUTLINE OF RESEARCH

An annular rail gap switch was designed for a self-breakdown voltage of 30kV, with air as the dielectric. The outer dimensions of the design had to conform with the architecture of a KrF laser that is currently under construction at the University of Alberta. A high voltage triggering circuit was also developed to provide a rapidly rising voltage pulse at the trigger electrode of the rail gap to initiate breakdown of the switch. Furthermore, three different trigger electrode geometries were designed and tested in the rail gap to determine the effects of different field stresses on jitter and inductance.

All possible polarity combinations were applied to the high voltage and trigger electrodes of the rail gap and the switching behavior was monitored for each case. Finally, the effects of photo-preionization from bare sparks on spark gap performance were also studied.

In order to become familiar with spark gap switching, inductance and jitter measurements were initially conducted on a 3-electrode spark gap which is currently employed in the KrF laser facility. This provided the background needed to modify the 3-electrode design into an annular rail gap configuration. Test results for the 3-electrode gap are included in this report to provide a standard against which the developed rail gap switch may be compared.

3.2 DESCRIPTION OF SPARK GAP DESIGN

Cross sections of the 3-electrode and annular rail gap designs are shown in figures 3-1 and 3-2, respectively. The different geometries of the two types of spark gaps called for a change in electrode curvature and gap spacing in the rail gap design. The minimum gap spacing in the rail gap is 3.175mm (1/8in) between the trigger electrode and each of the main electrodes. For the 3-electrode gap, the corresponding gap spacing is 1.5875mm (1/16in).

The large bodies of dielectric that surround the electrodes were designed to prevent arcing along the exterior of the gap. In the case of the rail gap, acrylic was chosen as the exterior dielectric so that the breakdown channels could be observed. The interior walls of the dielectric in the rail gap were tapered to increase the tracking distance, reduce effects of the dielectric on the electric field configuration, and also to reduce any pressure shock that the dielectric might receive during

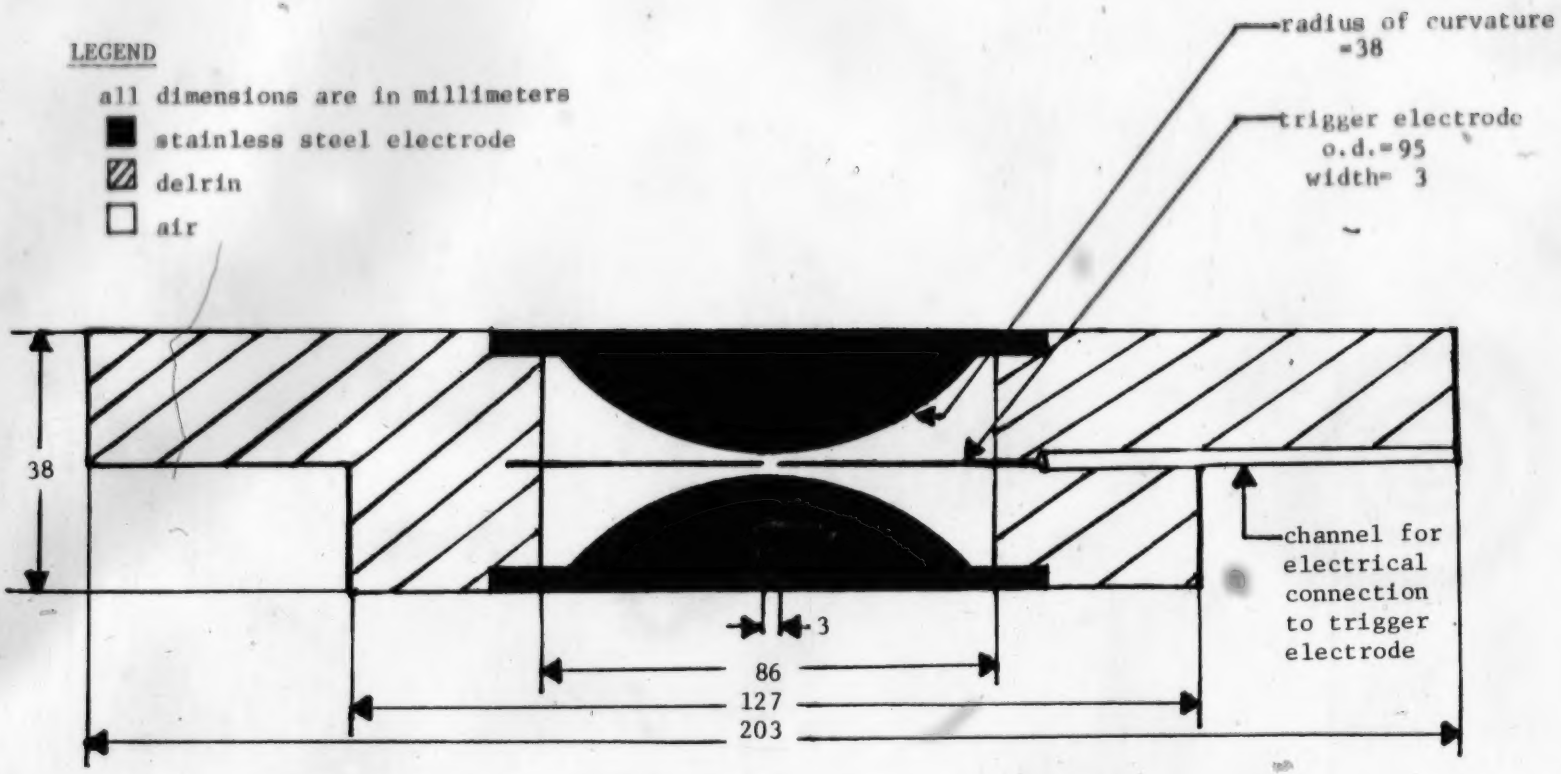

Figure 3-1. The 3-electrode Spark Gap Design.

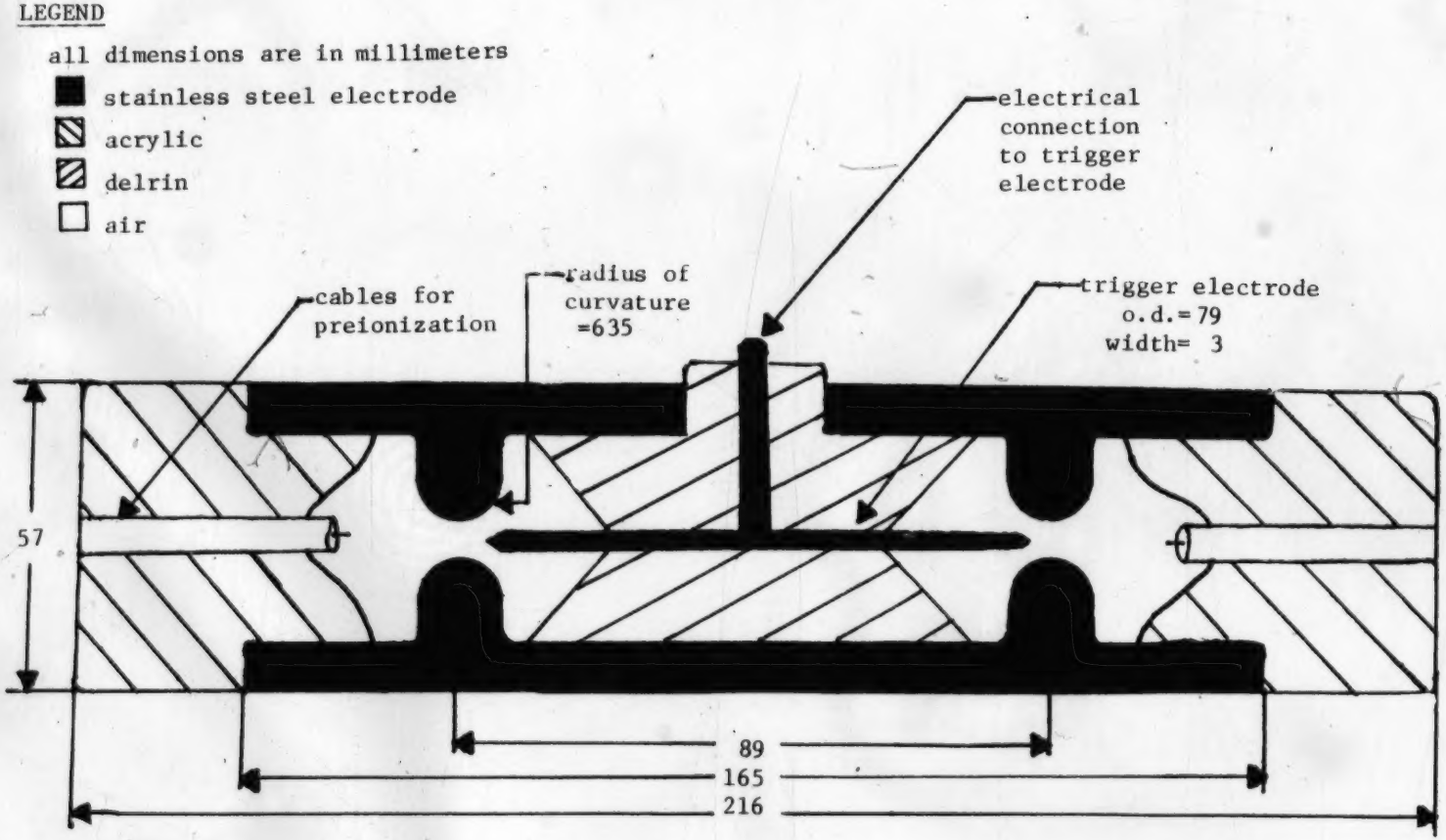

Figure 3-2. The Annular Rail Spark Gap Design.

spark breakdown.

Both spark gaps were sealed and polyethylene tubes were inserted into opposite sides of the gaps to allow for pressurization and air flow through the gap spacing. The rate of flow was sufficient to replace the small volume inside the gap with fresh air for each shot.

To provide the bare sparks for photo-preionization, four open ended coaxial cables were also symmetrically inserted into the rail gap, in the plane of the trigger electrode.

The geometry of the three trigger electrodes that were tested are shown in figure 3-3. The first is a standard blade edge electrode that is commonly used in linear rail gap designs. The second electrode has a duller edge than the blade electrode, and was designed to investigate the effects of reduced field stresses on the spark gap switching performance. The dull electrode may also be considered as a model for an aged blade electrode that has been rounded through erosion.

The third electrode in figure 3-3 has a sharp sawtooth edge. This geometry was tested to determine if localized field enhancement would increase the number of breakdown channels in the rail gap.

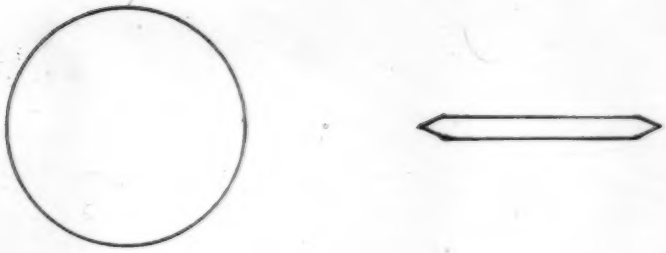

a. The Blade Electrode

b. The Dull Electrode

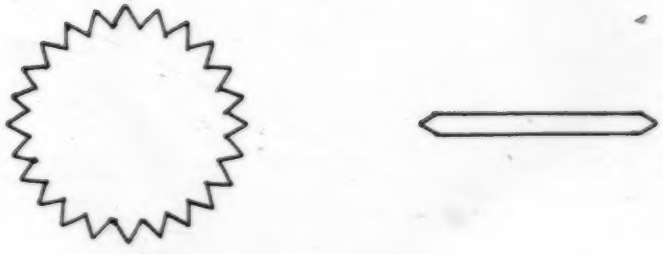

c. The Sawtooth Electrode

Figure 3-3. The Three Trigger Electrodes

3.3 DESCRIPTION OF CIRCUIT DESIGN

Circuit diagrams of the electrical and diagnostic arrangements for the 3-electrode and rail spark gap experiments are shown in figures 3-4 and 3-5, respectively. The high voltage electrode of the tested spark gap is maintained at a potential of ±30kV by the d.c. charged capacitor Ce. The trigger electrode of the spark gap is d.c. biased to half of the hold off voltage by two 100Mohm resistors. A high voltage pulse, sent to the trigger electrode, initiates breakdown of the gap. Closure of the spark gap results in an oscillatory discharge of Ce. The current of this discharge is monitored by a Rogowski coil.

3.3.1 CIRCUIT GEOMETRY

For the 3-electrode gap experiment, the capacitor Ce was electrically connected to the spark gap by a 3 inch wide copper plate. The spark gap was mounted and grounded to an earthed table by a 1/2 inch diameter steel stud bolt. The inductance of the stud bolt was measured to be approximately 17nH, and the inductance of the capacitor was rated at 20nH. Calculations indicated the inductance of the copper plate to be about 20nH. Hence, the total inductance of the circuit external to the spark gap was approximately 57nH.

To reduce circuit inductance in the annular rail gap experiment, the discharge circuitry was arranged into a tight coaxial-type geometry, as illustrated in figure 3-6. The capacitor bank (Ce in figure 3-5) was made up of five

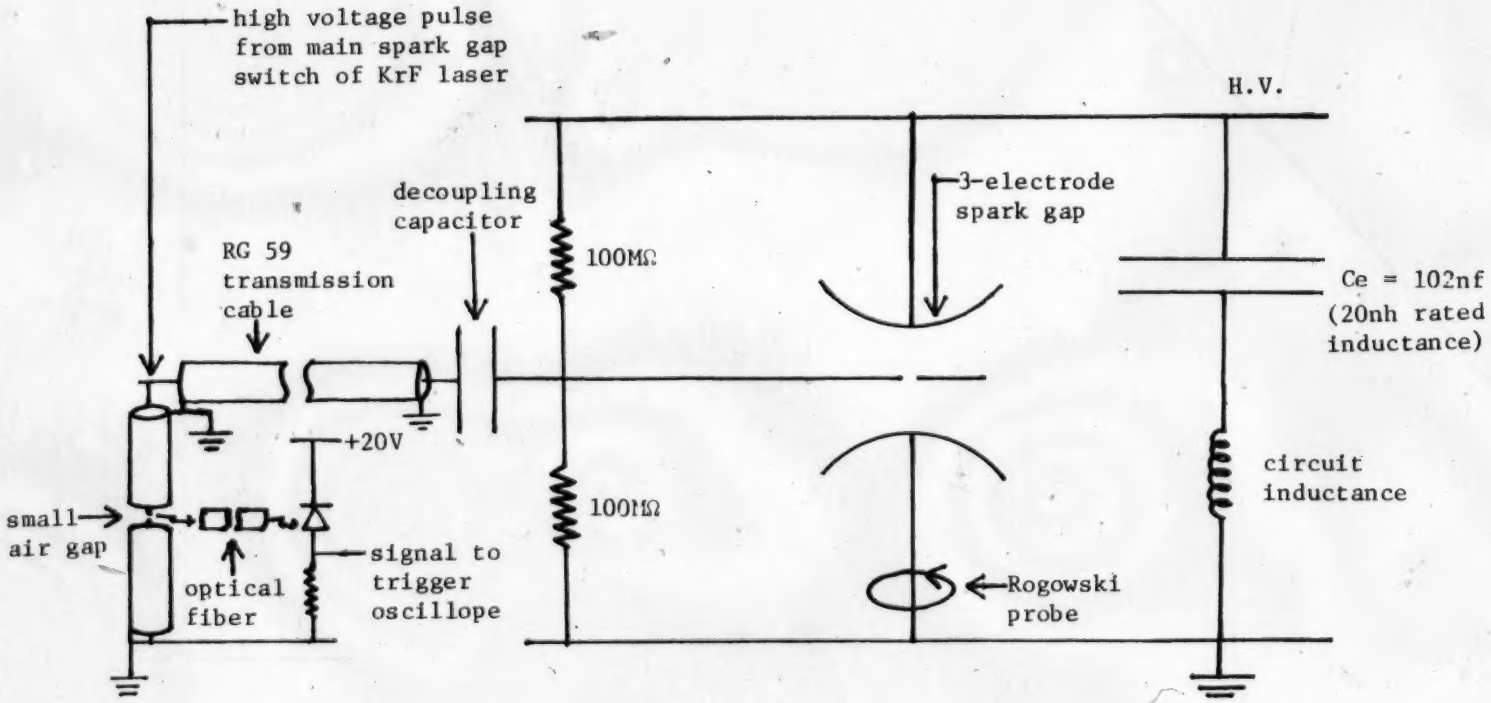

Figure 3-4. Circuit Diagram of the 3-electrode Spark Gap Experiment.

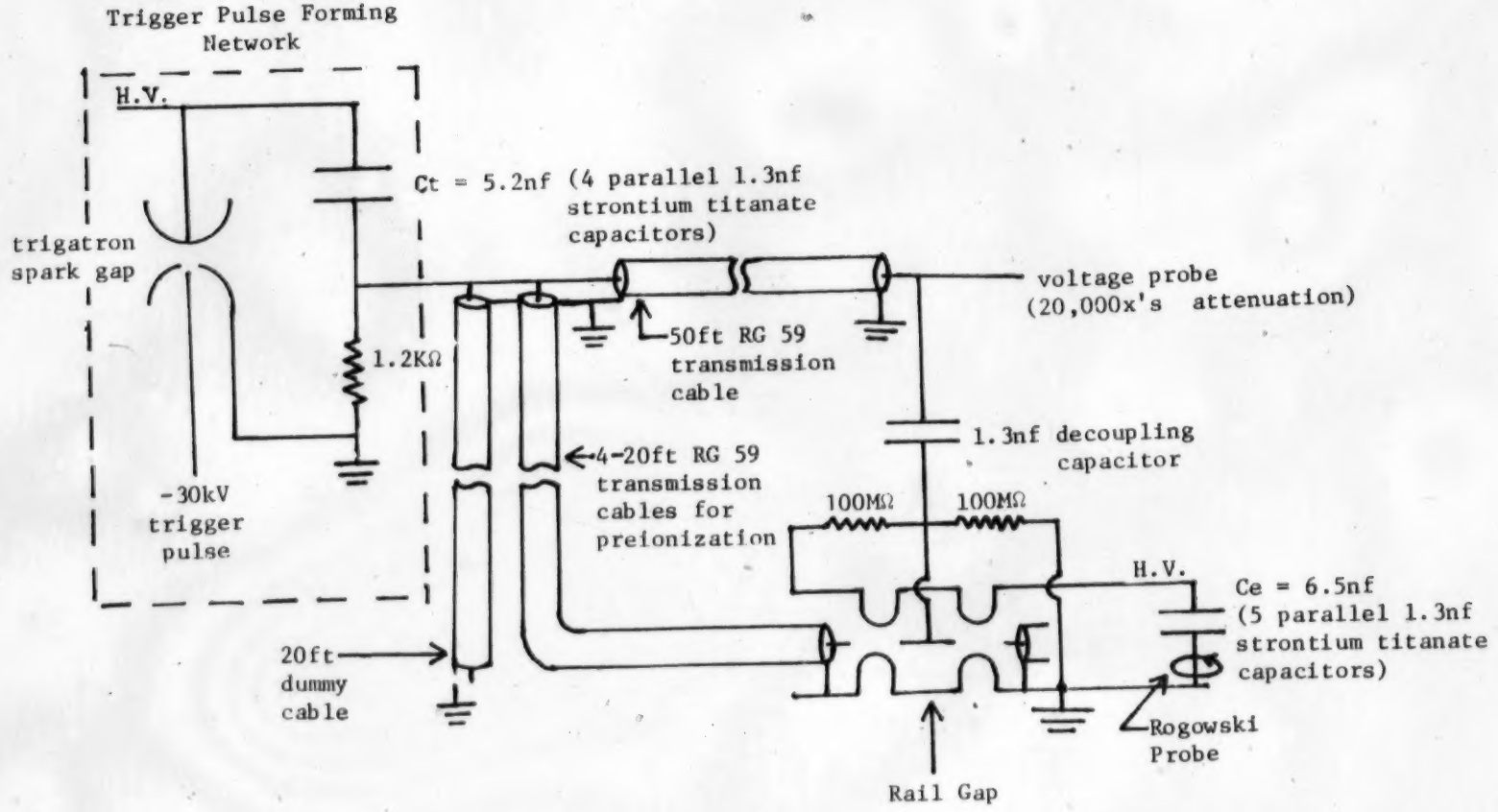

Figure 3-5. Circuit Diagram of the Rail Spark Gap Experiment.

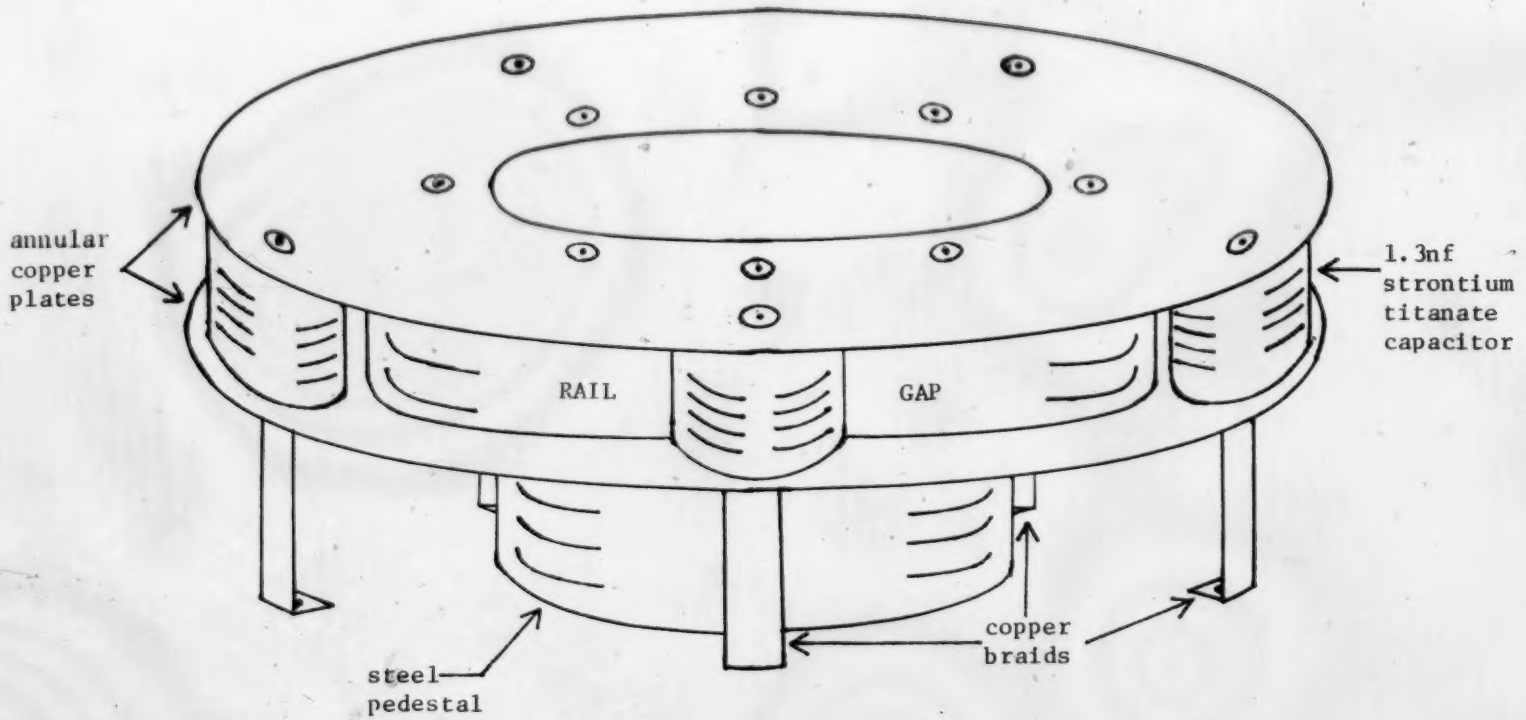

Figure 3-6. The Annular Rail Spark Gap Discharge Circuit Geometry.

strontium titanate capacitors which were symmetrically distributed around the gap. The capacitors in the bank were electrically connected by annular copper plates, one of which was also connected to the high voltage annular rail gap electrode. The other annular plate connected the capacitors to ground through five symmetrically distributed, three inch long copper braids (of rectangular cross section). An analysis of the inductance of this circuit geometry is included in Chapter 5.

3.3.2 TRIGGER PULSE CIRCUITRY

For tests on the 3-electrode spark gap, the trigger pulse was provided by a main spark gap switch which supplied synchronized triggering to the KrF laser facility. The loading on this switching circuit limited the pulse rate-of-rise to nominally 2kV/ns.

As part of the development of the rail spark gap test chamber, a separate trigger pulse forming network was constructed. This circuit is also shown in figure 3-5. A trigatron spark gap was employed to provide the high voltage switching for the trigger pulse. Breakdown of the trigatron gap was initiated by a high voltage pulse that was produced by the closure of an SCR switch. This allowed a charged capacitor to discharge into the primary of a step-up transformer. The SCR switch could be operated manually or automatically through an Intersil NE/SE-555 monolithic timing circuit that was designed to trigger the SCR

approximately every 6 seconds.

Closure of the trigatron spark gap produces an inverted capacitor voltage at the transmission lines. As the capacitor Ct discharges through the closed gap, a transient voltage pulse is sent down the six transmission lines, one of which is connected (through a decoupling capacitor) to the trigger electrode of the gap.

When the voltage pulse arrives at the ends of the transmission lines, the open circuit termination causes it to be reflected and doubled. In the case of the trigger pulse, the d.c. value of the charged decoupling capacitor is superimposed on the pulse voltage when it meets the trigger electrode. Accounting for a 1dB cable loss along the 50ft transmission line, the peak voltage at the trigger electrode can be expressed as:

$$V_o=-2V_1/1.25+V_2/2 \qquad (3.1)$$

where V_1 is the d.c. hold-off voltage of the trigatron spark gap and V_2 is the d.c. hold-off voltage applied to the rail gap.

The d.c. voltage for both the trigatron spark gap and the rail gap was provided by a single power supply. Consequently, changes in polarity of the rail gap would also mean a polarity change on the trigatron gap. A negative d.c. voltage across the trigatron spark gap affected the discharge performance in the trigatron spark gap, however, and reduced the smoothness and rate-of-rise of the transient

pulse. Switching of the trigger pulse polarity was achieved by reversing the leads at the end of the transmission cable.

3.3.3 OPERATING VOLTAGES AND PRESSURES

The operating d.c. voltage for both the trigatron spark gap and the rail spark gap was $\pm$30kV for all experiments. Application of equation 3.1 reveals the peak voltage for the trigger pulse at the trigger electrode to be $\pm$63kV when the pulse is of the same polarity as the rail gap hold-off voltage, and $\pm$33kV when the trigger pulse is of opposite polarity to the hold-off voltage.

It should be noted, however, that for either case the greatest potential difference between the trigger electrode and one of the main rail gap electrodes is 63kV. When the trigger pulse is of the same polarity as the applied d.c. hold-off voltage, there is a potential difference of 63kV between the trigger electrode and the grounded main electrode. Conversely, when the trigger pulse is of opposite polarity to that of the d.c. hold-off voltage, the 63kV potential difference is between the trigger electrode and the high voltage main electrode.

Preliminary tests of jitter vs rail gap pressure gave optimum results when the spark gap was operated just above the minimum hold-off pressure. Hence, operating pressures for the rail gap were chosen to be 27 PSIA for positive d.c. voltages, and 40 PSIA for the negative voltages.

A possible reason for the different hold-off pressures is that when the trigger electrode is negatively biased, the higher field stress at the trigger electrode makes it more susceptible to cold cathode emission which reduces the self-breakdown voltage[8]. An increase of pressure increases the sparking potential to above the chosen 30kV.

3.3.4 CIRCUITRY FOR PREIONIZATION

The remaining 5 transmission lines connected to the trigger pulse forming circuit were used in either of the following modes:

1. 4 of the 5 cables transferred high voltage pulses to induce breakdown of the small air sparks used for preionization. The fifth cable provided an extra access for any additional diagnostics that may be called for.
2. If no preionization or additional diagnostics were used, all 5 cables were replaced by dummy cables to keep a constant load on the trigger circuitry.

The open ends of the four cables that provided the photo-preionization were symmetrically inserted into the sides of the rail gap and allowed to spark with application of the voltage pulse. Each of these lines were 20ft long (compared with the 50ft transmission line that delivered the voltage pulse to the trigger electrode), so that there was a 45ns delay between the arrival of the voltage pulse at the ends of the preionization cables and the arrival of the voltage pulse at the trigger electrode. Preliminary

measurements showed a typical time lag of 20ns for the development of a spark at the open end of a high voltage transmission line. Hence the delay time between the preionization sparks and the arrival of the voltage pulse at the trigger electrode was nominally 25ns.

3.4 MEASUREMENT PROCEDURE AND DIAGNOSTICS

The discharge currents in the 3-electrode and rail gap experiments were monitored by a Rogowski coil that was placed on the grounded side of the discharge circuitry. An integrator was attached to the Rogowski coil in the 3-electrode experiment so that the current discharge could be monitored directly on the oscilloscope. However, in the case of the rail gap experiment, noise problems forced the removal of the integrator from the diagnostics. Consequently, the derivative of the discharge current, dI/dt, was monitored, which subsquently was digitized and numerically integrated for analysis.

The waveform of the discharge current was found to fit an underdamped series L-R-C circuit model which is illustrated in figure 3-7. Re, Le, and Ce are the resistance, inductance and capacitance of the discharge circuitry external to the spark gap, while Rg, Lg and Cg are the corresponding spark gap values. The spark gap capacitance Cg is of the order of 10pf and can therefore be neglected with respect to the external circuit capacitance. The inductance Lg and resistance Rg are those associated

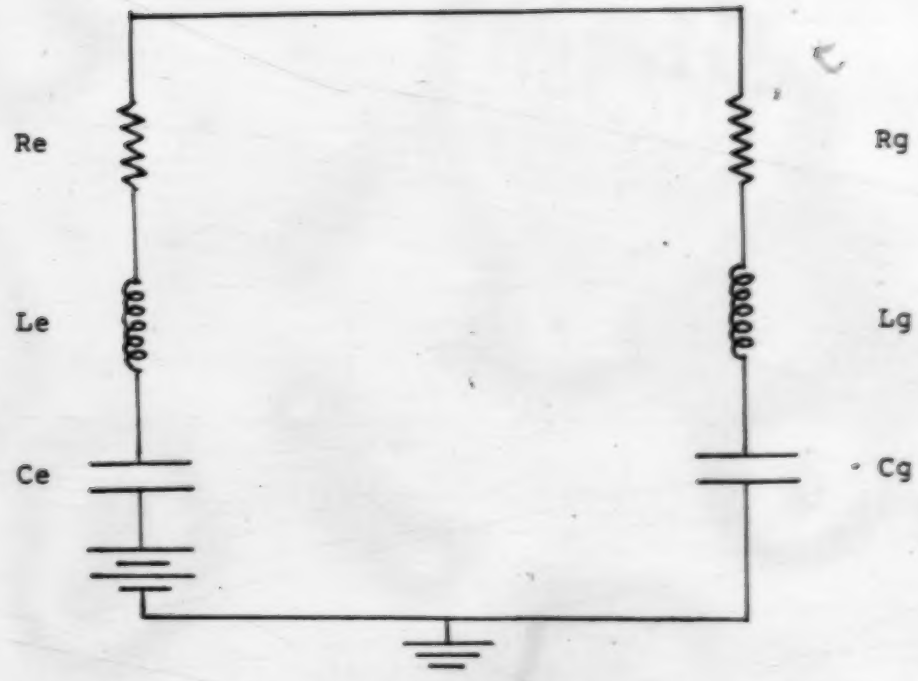

Figure 3-7. The L-R-C Equivalent Circuit Model of the Discharge Circuitry.

with the breakdown channels in the discharge.

The current response for an underdamped series L-R-C circuit is:

$$I=K\exp(-\beta\omega t)\sin[\omega(1-\beta^2)^{1/2})t] \qquad (3.2)$$

where

$$K=V_o/L\omega(1-\beta^2)^{1/2} \qquad (3.3)$$

$$\omega=(LC)^{-1/2} \qquad (3.4)$$

$$\beta=R(C/L)^{1/2}/2 \qquad (3.5)$$

R, L, and C are the total series resistance, inductance and capacitance of the circuit, and V_o is the intial d.c. voltage across the charged capacitor. If $\beta<1$, then the period T of the sinusoid is approximately equal to $2\pi/\omega$. Hence, the inductance of the circuit can be determined directly from the period of the discharge through the relation:

$$L=T^2/(4\pi^2C) \qquad (3.6)$$

Jitter measurements were achieved in the following manner. A signal, sent simultaneously with the voltage pulse travelling to the trigger electrode of the gap, was used to externally trigger an oscilloscope. Differences in the arrival times of the discharge current signals at the oscilloscope were noted for typically 100 shots, and a standard deviation was calculated. In addition, in the case of the rail gap, typical breakdown delay times were recorded.

For the 3-electrode gap experiment, the external trigger for the oscilloscope was provided by an optical signal that was generated by plasma emission produced by breakdown of a small air gap - caused by a high voltage signal from the main spark gap switch (figure 3-5). In the case of the rail gap, a voltage signal was taken from the spark gap trigger pulse just before it reached the trigger electrode. In addition to providing a method of monitoring the voltage pulse to the electrode, this signal was used (in place of the optical signal) to provide the external trigger for the oscilloscope. This procedure eliminated the added jitter (typically a 2ns window) induced by the randomness in time of breakdown of the small air gap, and therefore provided more reliable data. The voltage signal from the trigger electrode was attenuated 20,000 times before it was sent to the oscilloscope. The total risetime of the voltage probe and divider circuitry was 6ns.

4. RESULTS OF THE 3-ELECTRODE SPARK GAP EXPERIMENT

The results obtained from jitter measurements and inductance calculations for the 3-electrode spark gap experiment are presented in this chapter.

4.1 INDUCTANCE AND RESISTANCE OF THE 3-ELECTRODE SPARK GAP

A typical oscillogram showing the current waveform from the 3-electrode spark gap discharge circuitry is illustrated in figure 4-1. The sinusoidal waveform has a period of 640ns. Knowledge of this period and the circuit capacitance of 102nf when applied to equation 3.6 (assuming $\beta<1$) reveals a total circuit inductance of 102nH. The circuit inductance external to the 3-electrode gap was calculated to be approximately 57nH. Hence, the inductance of the 3-electrode gap is determined to be nominally 45nH.

The intrinsic resistance associated with the 3-electrode gap discharge can be found from a comparison of the amplitudes of successive peaks in figure 4-1. From equation 3.2 the ratio of the amplitudes of the peaks (at the times t_1 and t_2), leads to the relation:

$$I(t_1)/I(t_2)=\exp[-\beta\omega(t_1-t_2)]=6.8/4.4=1.5 \qquad (4.1)$$

Hence, for

$$t_2-t_1=2\pi/\omega; \qquad (4.2)$$

$$\beta=\ln[I(t_1)/I(t_2)]/\omega(t_2-t_1)=\ln(1.5)/2\pi=.065 \qquad (4.3)$$

The assumption that $\beta<1$ is valid. Substituting this value into equation 3.5, and solving for R gives R=0.13 ohm.

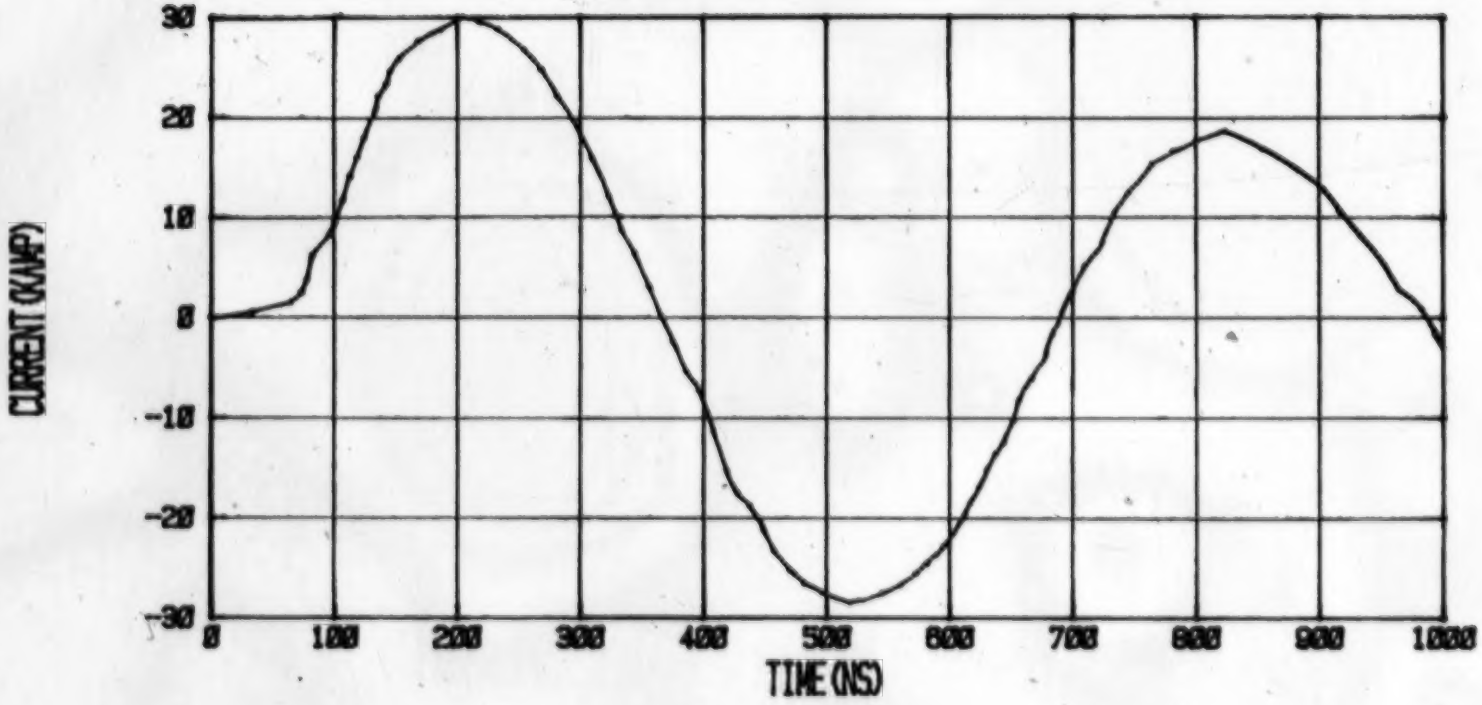

Figure 4-1. Current Waveform of the 3-electrode Gap Discharge Circuit.

4.2 JITTER MEASUREMENTS OF THE 3-ELECTRODE SPARK GAP

The minimium jitter for the 3-electrode gap was determined to be 1.2ns (smd). In this particular case, the d.c. voltage that was applied to the gap was +30kV and the gap pressure was 45PSIA. The peak voltage of the trigger pulse was approximately -45kV.

The above result does not, however, account for the 2ns window jitter of the small air gap which was the source of the optical signal that was used to externally trigger the oscilloscope. Assuming a Gaussian distribution for this jitter, 95% of the 2ns window can be represented by 4 times the standard mean deviation of the intrinsic jitter of the optical source. Incorporation of the .5ns smd for the optical signal into the calculated spark gap jitter reveals an intrinsic jitter for the 3-electrode gap of 1.1ns.

4.3 CONCLUSIONS OF THE 3-ELECTRODE SPARK GAP EXPERIMENT

The 3-electrode spark gap switch was found to have an intrinsic inductance of 45nH. The minimum breakdown jitter of the 3-electrode gap was determined to be 1.1ns. These results show that the 3-electrode spark gap may be very useful for high voltage switching applications where small jitter times are essential. However, the relatively large inductance that is associated with this type of spark gap configuration does not make it very practical for applications where very fast switching is called for.

5. RESULTS OF THE ANNULAR RAIL SPARK GAP EXPERIMENT

This chapter outlines the results from the tests that were conducted on the rail gap design. The first section discusses the waveforms that were obtained from voltage and current diagnostics. This is followed by some examples of how the breakdown delay and jitter times were measured. The next section describes the calculations of the rail gap inductance. The final results of the experiment for the blade, dull and sawtooth electrodes are listed in tables 5-1 to 5-3. A discussion of these results concludes this chapter.

5.0.1 DEFINITIONS OF ADOPTED NOTATION

In the following discussion, a notation has been adopted for easy referral to the polarity combinations that were applied to the rail gap for each individual experiment. A particular polarity combination will be denoted by two signs, separated by a slash. The first of the two signs indicates the polarity of the spark gap d.c. hold-off voltage. The second sign indicates the polarity of the voltage pulse that is sent to the rail gap trigger electrode.

Where applicable, the suffix 'p' or 'np' denotes whether preionization or no preionization was applied to the gap for an individual experiment. For example, the notation +/-np refers to a positive d.c. hold-off voltage and a negative trigger pulse, with no preionization.

5.1 DISCUSSION OF OBSERVED WAVEFORMS

Figures 5-1 to 5-5 show characteristic waveforms that were observed in the rail gap experiments, when a blade, dull or sawtooth trigger electrode was employed. Each waveform corresponds to a particular polarity combination, with or without the use of preionization. Examination of the waveforms (particularly the trigger pulse waveforms) show every case to be unique. However, for each individual experiment, the only differences that were found in the oscillograms from shot to shot were the delay times corresponding to each stage of breakdown, as well as small changes in the periods of the discharge.

Figures 5-1 to 5-5 illustrate some of the the trigger voltage pulses that were seen at the end of the 50ft transmission line, before passing through the charged decoupling capacitor to the trigger electrode of the gap. Consequently, the added d.c. biasing voltage across the decoupling capacitor is not shown. When the biasing voltage is added to the voltage seen in the oscillograms, the peak trigger pulse voltage value corresponds well with that predicted by equation 3.1.

Figure 5-1 shows the trigger voltage pulses that were observed when a +/- polarity combination was applied to the rail gap and blade electrode. The leading edge of the voltage pulse is smooth and reaches its peak value in 8ns.

Figure 5-2 illustrates an example of the noise level that was observed with the trigger voltage pulse when

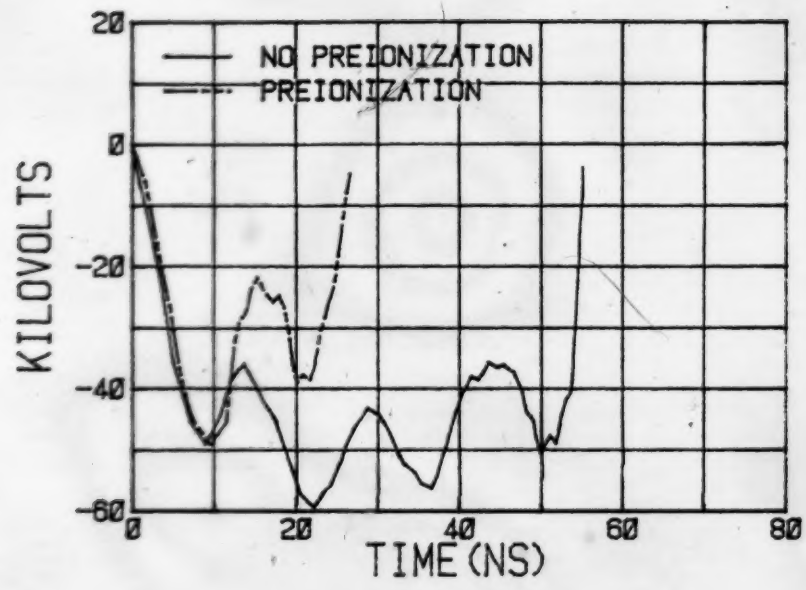

Figure 5-1. Observed Trigger Voltage of the Rail Gap Experiment with a Blade Trigger Electrode and +/- Polarity Combination.

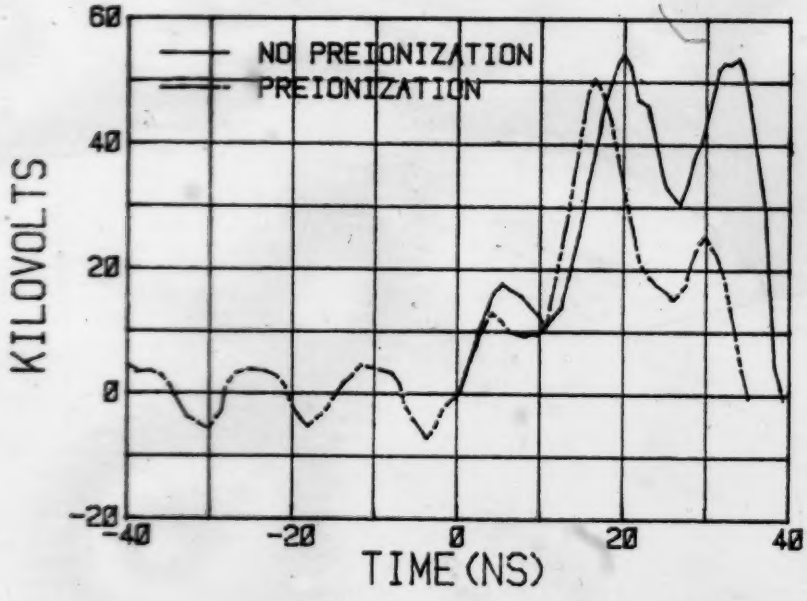

Figure 5-2. Observed Trigger Voltage of the Rail Gap Experiment with a Blade Trigger Electrode and +/+ Polarity Combination.

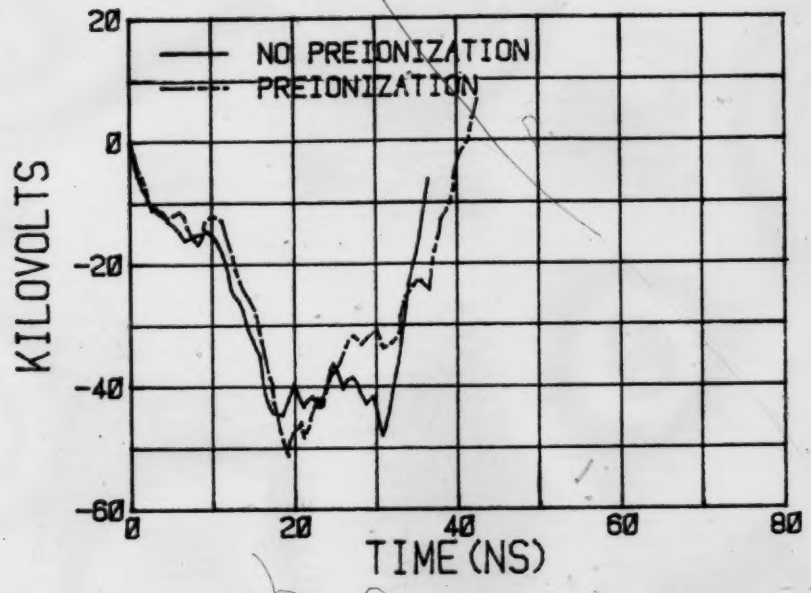

Figure 5-3. Observed Trigger Voltage of the Rail Gap Experiment with a Sawtooth Trigger Electrode and -/- Polarity Combination.

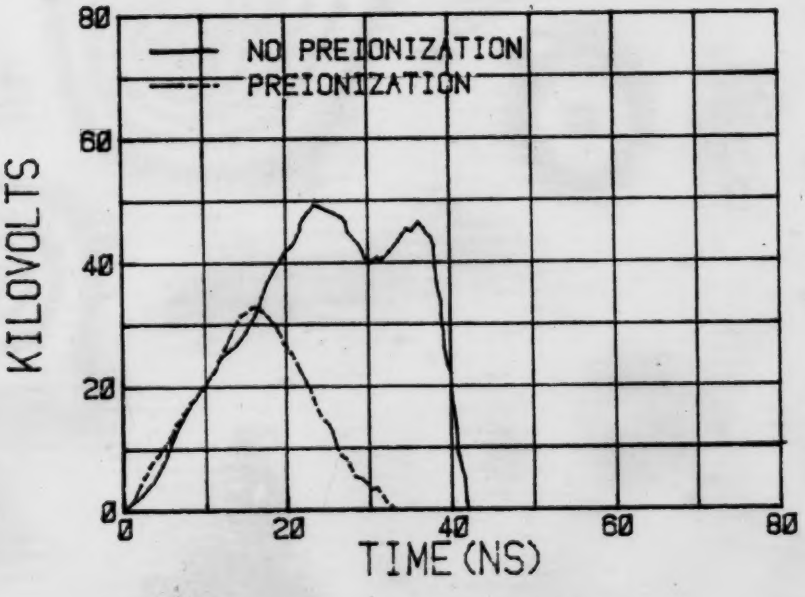

Figure 5-4. Observed Trigger Voltage of the Rail Gap Experiment with a Dull Electrode and +/+ Polarity Combination.

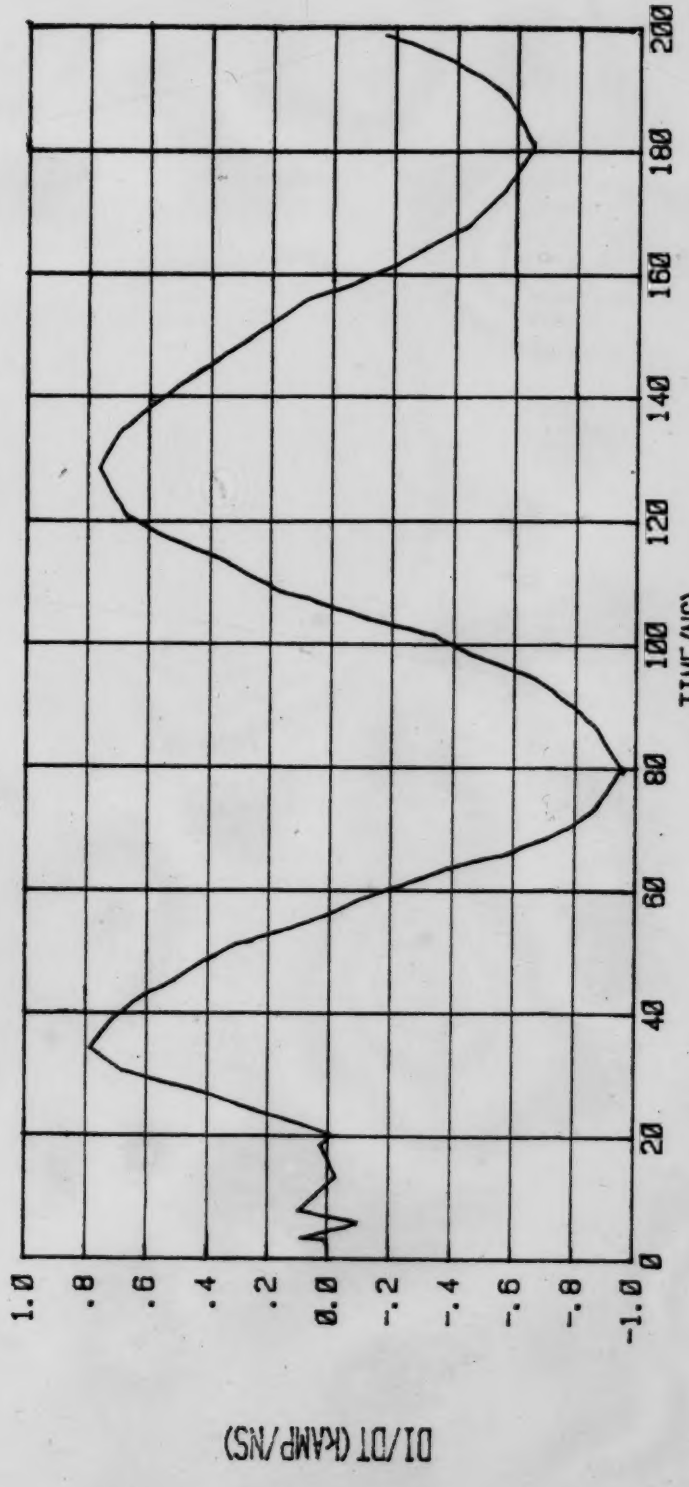

Figure 5-5. The Discharge Current Differential with Respect to Time that was Observed when a +/+p Polarity was Applied to the Rail Gap and Sawtooth Trigger Electrode.

preionization was applied to the gap. The zero on the time scale corresponds to the reference point from which the time to peak voltage was measured. Although this much noise was not usually observed prior to the leading edge of the voltage pulse, it does add some uncertainty to the true quality (smoothness, risetime and peak voltage value) of the voltage pulse at the trigger electrode; it may also account for some of the bumps that were seen in the other waveforms.

The deterioration of the leading edge of the voltage pulse where the spark gap hold-off voltage is negative (as shown in figure 5-3) is probably due to the asymmetrical position of the trigger electrode in the trigatron spark gap. When this trigger electrode sparks over to the grounded electrode, the free electron density (resulting from the sparkover) is on the anode side of the gap. In this case the triggering of the spark gap is not as effective as it would be if the trigger electrode were to spark over to the cathode. The risetime of the current is decreased or deformed by the more slowly developing avalanches that fade and then reignite as they progress across the gap. Consequently, a slower risetime - as well as humps in the rising edge - is seen in the voltage pulse when the applied hold-off voltage is negative.

Because of the variations of the leading edge of the trigger voltage waveforms, a fair evaluation of the rate-of-rise was difficult to assess. The trigger pulse rate-of-rise was determined from the ratio of the change in

voltage at the trigger electrode, to the time for the observed pulse to meet its peak value. For example, for the +/-np blade electrode case, the trigger voltage rate-of-rise was determined to be 48kV/8ns or 6kV/ns. In the -/-np sawtooth electrode case the rate-of-rise was 48kV/17ns or 2.8kV/ns.

The falling edge of the trigger pulse shows the time of the first breakdown stage, corresponding to the voltage transition of the trigger electrode. Comparison of the trigger voltage waveforms, for each polarity combination, clearly show that this delay time is reduced when preionization is applied to the gap. In particular, figure 5-4 illustrates a case where preionization causes the first breakdown stage to occur prior to peak voltage of the trigger pulse.

A typical example of the observed discharge current differential with respect to time, dI/dT, is shown in figure 5-5. However, for greater resolution of the periods and breakdown delay times, only the first period of the sinusoid was usually monitored in each observation. Figure 5-6 illustrates characteristic current discharge waveforms (and corresponding breakdown delay times) that were obtained from digitization and numerical integration of dI/dT oscillograms. The waveforms shown here were chosen to represent the typical breakdown performance of the rail gap when the blade, dull or sawtooth trigger electrode was employed. Since the Rogowski coil used to obtain these

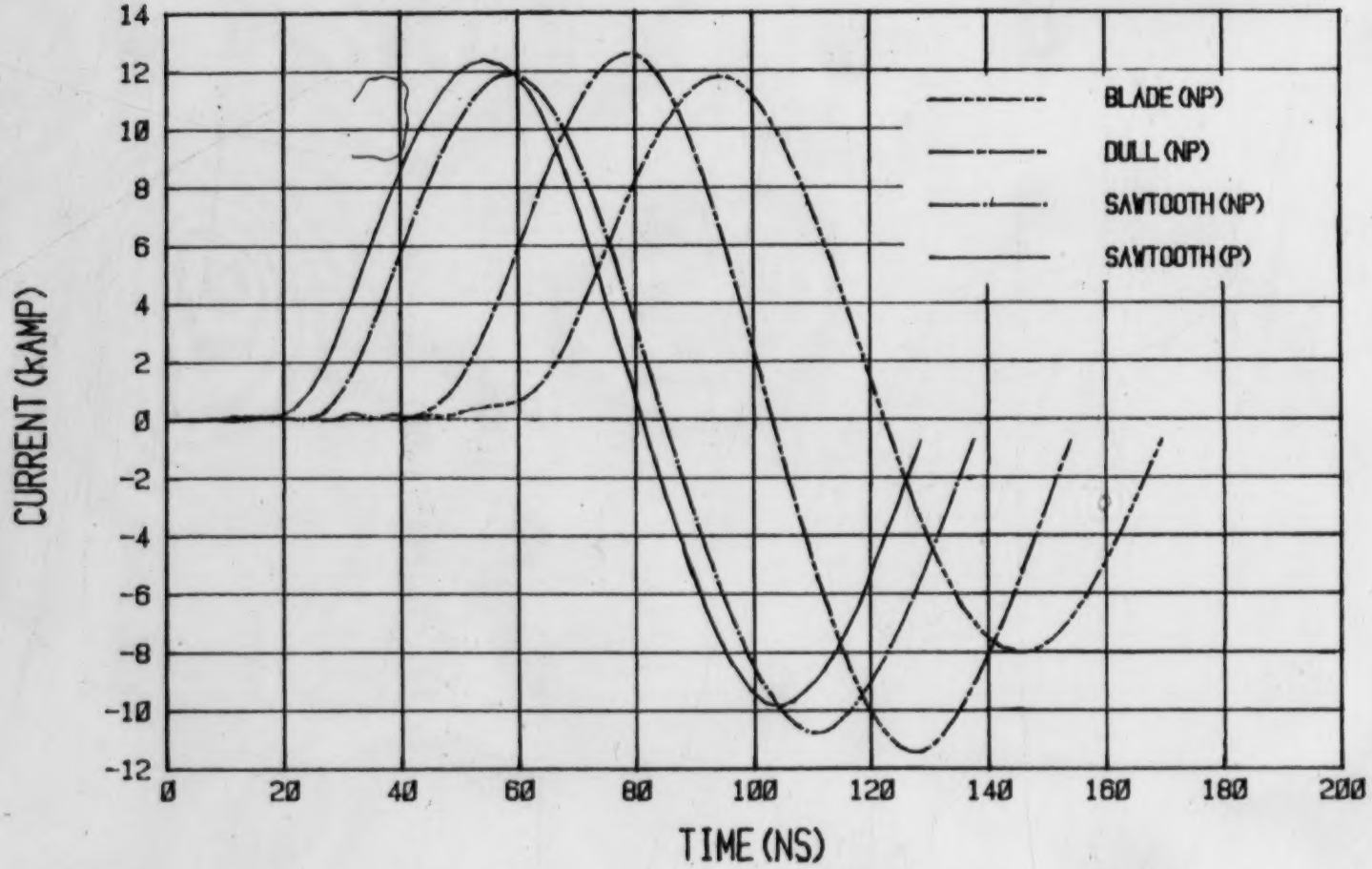

Figure 5-6. Characteristic Current Discharge Waveforms when a +/+ Polarity Combination is Applied to the Rail Gap and Blade, Dull and Sawtooth Trigger Electrodes.

measurements was not calibrated, the exact quantities of dI/dt were not observed. The amplitudes of the sinusoids in figures 5-5 and 5-6 were calculated from equation 3.2 and its derivative.

5.1.1 CALCULATIONS OF DELAY AND JITTER TIMES

All delay times were taken with respect to the time of peak voltage of the trigger pulse. The delay time for the first breakdown stage corresponds to the time that the trigger pulse falls from its peak voltage value. For example, in the +/-np case with the blade electrode (figure 5-1), the delay time to the first breakdown stage was found to be typically 42ns. When preionization was applied with this polarity combination, the first stage delay time was reduced to 12ns.

The overall breakdown delay times were measured by the appearance of the sharp rising edge of the sinusoids in the observed dI/dt waveforms. These delay times were monitored on the oscilloscope with respect to the rising edge of the trigger pulse as described in section 3.4. A 10ns diagnostic cable delay time as well the trigger pulse rise time were subtracted from the observed delay times to give the final results. For example, in the +/+p sawtooth electrode case, the observed overall delay time was 48ns. The time to peak voltage of the trigger pulse was 18ns. Subtraction of the voltage risetime and the 10ns cable delay time reveals an overall breakdown delay time of 20ns (figure 5-6).

As described in section 3.4, the jitter measurements were obtained by monitoring the change in the breakdown delay times over a number a shots, and the standard mean deviation was calculated. This method was used to find the total breakdown jitter, as well as the jitter of the first breakdown stage. In the +/-np blade electrode experiment the standard mean deviation in the delay time of the first breakdown stage was 10.1ns. The total breakdown jitter was 10.9ns.

5.1.2 RAIL SPARK GAP AND EXTERNAL DISCHARGE CIRCUIT INDUCTANCE CALCULATIONS

The sinusoidal waveforms in figure 5-6 show that the spark gap discharge current conforms to the current model that was described section 3.4. Apart from inaccuracies created by digitization and numerical integration of the observed dI/dt's, periods taken from different parts of a particular sinusoid are seen to be relatively constant. However, oscillograms of a number of superimposed shots showed that the discharge period would vary by as much as 4ns for each individual experiment.

Since the zeroes of dI/dt correspond to the peaks of the current discharge, the period of a sinusoid can be determined directly from the observed waveforms as twice the time between the second and third zeroes of dI/dT. This process eliminates the uncertainties that are added in the waveform digitization and numerical integration. Because the

rail gap inductance is relatively small, it is important that additional errors in the inductance calculations be kept to a minimum.

To check the simplified relationship between T, L, and C (equation 3.6), we must establish that the value of β in equation 3.2 is much less than 1. Assuming this to be true, then differentiation of equation 3.2 gives:

$$dI/dt=K\omega\exp(-\beta\omega t)\cos[\omega(1-\beta^2)^{1/2}t] \qquad (5.1)$$

The value of β can be calculated from the ratio of the heights of the second and third extrema in dI/dt, through a relation similar to that of equation 4.3:

$$\beta=1/\pi\ln\{[dI(t=t_1)/dt]/[dI(t=t_2)/dt]\} \qquad (5.2)$$

where t_1 is the time of the second extrema and t_2 is the time of the third extrema in the sinusoid.

For the +/+np blade electrode experiment, analysis of the observed waveform, dI/dt, revealed that $[dI(t=t_1)/dt]/[dI(t=t_2)/dt]=5.4/4.2=1.3$. Substitution of these values into equation 5.2 gives a β of 0.08. Figure 5-6 shows the blade electrode case to have the largest damping of the three trigger electrodes that were tested. Hence, β is much less than one for all cases and the circuit inductance can be determined directly from the period of the observed discharge, using equation 3.6. For the +/+np blade electrode case, application of the 104ns period to equation 3.6 leads to a total circuit inductance of 42nH.

To determine the inductance of the circuit external to the rail gap, periods of the sinusoidal discharge were compared for a different number of capacitors and braids. The inductance of each strontium titanate capacitor was determined to be 51nH, with an uncertainty of $\pm$3nH. Unfortunately, calculations of the braid inductance were not as consistent. This inconsistency can be attributed to a lack of uniformity in the copper braids, as well as to the effect of different loads on the rail gap which may vary its intrinsic inductance. At any rate, an average value for the inductance of the copper braids was determined to be 110nH with an uncertainty of $\pm$15nH. Since the external circuit was made up of 5 parallel capacitors in series with 5 parallel copper braids, the net external circuit inductance is 32$\pm$6.8nH. This result indicates an intrinsic rail gap inductance of 10nH for the +/+np case with the blade electrode.

The 4ns changes in the periods of the sinusoids from shot to shot reveals an additional uncertainty in the inductance calculations. Consideration of this uncertainty, as well as a possible 2ns error in the reading of the oscillograms, leads to an added uncertainty of 4nH in the rail gap inductance. Hence the total error in the spark gap inductance calculations (including the uncertainty of the external circuit inductance) is determined by the sum of the squares of the individual errors to be $\pm$8nH.

In summary, for each experiment, the total circuit inductance was calculated (according to equation 3.6) from the periods of the observed waveforms dI/dt. A value of 32nH was subtracted from the total inductance to account for contributions of the circuit external to the spark gap. The final results of the calculated rail gap inductance for each experiment are listed in tables 5-1 to 5-3. The total uncertainty of these results is $\pm$8nH.

5.2 DISCUSSION OF RESULTS

Typical delay times, as well as jitter and inductance results of the tests that were conducted on the annular rail gap design with a blade, dull and sawtooth edge electrode are listed in tables 5-1 to 5-3, respectively. The results show a wide range of values over all of the measurements that were taken. Although the blade edge electrode is most commonly used in spark gap applications, it is seen here to give the highest average inductance and jitter of the three trigger electrodes that were tested. The dull electrode has reduced inductance in every case when compared with the blade electrode, and improved overall jitter in every case except for +/-np. The sawtooth electrode demonstrates the lowest average jitter, as well as the lowest average inductance with preionization.

Preionization is seen to improve both inductance and jitter for most cases. The greatest effect of preionization is found in the first breakdown stage where the delay times

Table 5-1. Delay, Jitter and Inductance Results of the Annular Rail Gap with a Blade Trigger Electrode.

Case	Trigger Voltage Rate-of-Rise (kV/ns)	Delay to First Breakdown Stage (ns)	Delay to Complete Breakdown (ns)	Jitter of First Breakdown Stage (smd)	Overall Jitter (smd)	Jitter Improvement with Preionization (%)	Calculated Rail Gap Inductance (nH)
+/-np	6.0	42	60	10.1	10.9	86	17
p	6.0	12	40	0.5	1.5		10
+/+np	2.7	30	60	5.0	8.1	86	10
p	2.7	13	35	0.4	1.1		10
-/+np	3.2	35	135	8.7	42.2	92	17
p	2.2	15	120	0.9	3.4		15
-/-np	2.4	15	80	2.7	3.9	-10	9
p	1.4	3	65	0.8	4.3		10
Averages:							
np	3.6	30.5	83.8	6.6	16.3	84	13.3
p	3.1	10.8	65.0	0.7	2.6		11.3

Table 5-2. Delay, Jitter and Inductance Results of the Annular Rail Gap with a Dull Trigger Electrode.

Case	Trigger Voltage Rate-of-Rise (kV/ns)	Delay to First Breakdown Stage (ns)	Delay to Complete Breakdown (ns)	Jitter of First Breakdown Stage (smd)	Overall Jitter (smd)	Jitter Improvement with Preionization (%)	Calculated Rail Gap Inductance (nH)
+/-np	3.2	<3	25	3.8	4.0	0	12
p	3.2	occurred before peak voltage	20	<0.2	4.0		9
+/+np	2.4	15	45	4.7	5.1	86	5
p	1.9	occurred before peak voltage	25	<0.2	0.7		5
-/+np	2.4	35	65	10.5	30.0	95	13
p	6.0	12	60	0.5	1.5		12
-/-np	2.2	25	85	3.7	3.6	53	5
p	2.2	<3	70	1.0	1.7		5
Averages:							
np	2.6	<19.5	55.0	5.7	10.7	81	8.8
p	3.8	<3.8	43.8	0.4	2.0		7.8

Table 5-3. Delay, Jitter and Inductance Results of the Annular Rail Gap with a Sawtooth Trigger Electrode.

Case	Trigger Voltage Rate-of-Rise (kV/ns)	Delay to First Breakdown Stage (ns)	Delay to Complete Breakdown (ns)	Jitter of First Breakdown Stage (smd)	Overall Jitter (smd)	Jitter Improvement with Preionization (%)	Calculated Rail Gap Inductance (nH)
+/-np	6.0	15	30	7.6	8.8	93	10
p	6.0	<3	20	0.5	0.6		4
+/+np	2.7	5	25	0.5	1.6	19	9
p	2.7	<5	20	0.8	1.3		6
-/+np	1.7	25	80	7.0	5.2	65	17
p	2.2	15	50	0.9	1.8		15
-/-np	2.8	15	75	1.7	12.4	58	5
p	2.4	<3	60	1.0	5.2		4
Averages:							
np	3.3	15.0	52.5	4.2	7.0	69	10.3
p	3.3	<6.5	37.5	0.8	2.2		7.3

and jitter (with the exception of the +/+np sawtooth trigger electrode case) are dramatically reduced. Averages over the results for all three electrodes show that the overall delay times are reduced by an average of 15ns with preionization. The overall jitter is improved by an average of 80% with preionization, while the inductance is reduced by 19%.

Less improvement in overall jitter and inductance with preionization is generally seen for -/- cases. The -/- blade electrode experiment suggests that preionization may even worsen the spark gap switching performance, although the results with and without preionization for this case are so close that the discrepancies may simply be due to statistical error. At any rate, the -/+ results for the blade and dull electrodes (and the +/- case with the sawtooth electrode) clearly demonstrate how bad spark gap jitter can be dramatically improved with preionization.

The inductance of the rail gap ranges from 4nH in the case of the sawtooth electrode with preionization, to 17nH for the bladed electrode without preionization. The overall average inductance of the rail gap without preionization is 10.8nH, which is slightly under 1/4 of the inductance of the 3-electrode gap. This is an interesting result in that 3 to 5 spark channels were usually observed in the rail gap discharge. The average rail gap inductance with preionization is 8.8nH.

Some trends do appear with the different polarity configurations although few of them were really definitive.

For example, the -/+np combination shows high jitter characteristics for the blade and dull electrodes, although the jitter is quite reasonable for the sawtooth electrode. Conversely, relatively low jitter is seen in the -/-np case for both the blade and dull electrodes, but it is high for the corresponding case with the sawtooth electrode.

The trigger pulse rate-of-rise is generally found to be highest for the +/- polarity combination. This is a reasonable result because the hold-off voltage on the trigatron spark gap is negative. Since the quality of the trigger voltage pulse does affect spark gap switching performance[12], the high jitter of the +/-np configurations is an unexpected result. Furthermore, the jitter is higher in this case for the blade and sawtooth electrodes where the voltage rate of rise is 5-6kV/ns, than in the dull electrode case where the voltage rate-of-rise is only 3.2kV/ns.

In general, the results indicate that without preionization, rail gap inductance and jitter is lower for configurations where the trigger pulse is of the same polarity as the voltage applied across the main electrodes of the spark gap. The reduction of the inductance is especially significant in these cases. This result appears to be independent of the rate-of-rise of the trigger pulse and the different pressures that were used for the two hold-off voltage polarities. The +/+ polarity configuration with preionization provides low jitter, as well as reasonably low inductance for all three electrodes.

Figure 5-6 illustrates a comparison of the rail gap inductance and overall breakdown delay times for the three trigger electrodes that were tested. Based on the foregoing discussion, results from the +/+ polarity combination were chosen to represent each electrode. Since the inductance of the rail gap did not change with preionization for this polarity combination in the blade and dull electrode cases, only the current discharge of the sawtooth electrode experiment with preionization is shown in figure 5-6.

Due to the relatively small variations in the periods of the current discharge, direct comparison of the rail gap inductance from the periods is not very revealing in figure 5-6. However, from equations 3.2 to 3.4, the total inductance of the discharge circuitry is inversely proportional to the square of the amplitude of the sinusoid. Hence, comparison of the amplitudes of the first peaks in the waveforms in figure 5-6 may be considered as a more direct method of evaluating the rail gap switching performance for each trigger electrode.

The lowest jitter values are provided by the sawtooth electrode. These are 1.6 ns for the +/+ polarity combination without preionization, and 0.6ns for the +/-polarity with preionization. A minimum inductance of 4nH with preionization is found for the +/- and -/- cases of the sawtooth electrode. Minimum inductance of 5nH without preionization is noted for the -/- case of the sawtooth electrode, although it is also seen for the +/+ and -/-

cases with the dull electrode.

6. CONCLUSIONS

This research has demonstrated the performance of an annular rail spark gap design that has both low inductance and low jitter characteristics. Jitter measurements as low as 1.6ns without preionization and 0.6ns with the use of preionization (from bare sparks) were observed from the rail gap discharge when a sawtooth trigger electrode geometry was used. These results are comparable with the low jitter (1.1ns) characteristics of the 3-electrode spark gap.

Minimum inductances of 5nH without preionization and 4nH with preionization were also observed from the rail gap discharge when the sawtooth trigger electrode was employed. This is a significant improvement from the 45nH inductance of the 3-electrode gap.

The circuit inductance external to the rail gap was determined to be approximatey 32nH. Although efforts were made in the circuit design and construction to reduce the external inductance to a minimum, this value is clearly too high for optimum benefits of the rail gap design in a practical application. This implies that coaxial circuitry must be employed to derive the maximum benefits of a low inductance rail gap switch.

Results from the experiment showed that utilization of preionization, through the simple and inexpensive method of allowing non-terminated transmission cables to spark inside the gap prior to triggering, can dramatically reduce bad jitter characteristics with the added bonus of a slight

reduction in the spark gap inductance.

For this annular rail gap design, it was found that either a sawtooth or dull edge trigger electrode provided lower overall jitter and inductance compared to the standard blade edge electrode. Furthermore, the dull electrode supplied the lowest average inductance without preionization. These conclusions and the varying results for each polarity configuration clearly demonstrate the unpredictable nature of spark gap switching.

The spark gap discharge performance was generally optimum when a +/+ polarity combination was used, and this result appeared to be independent of the quality of the trigger voltage pulse employed. This indicates that other parameters (such as space-charge effects) also determine spark gap switching behavior.

Since the quality of the trigger pulse is known to affect spark gap switching performance, the jitter results may possibly be improved further with a faster and higher amplitude trigger pulse. It would be interesting to measure the rail gap jitter if another rail gap was employed to replace the trigatron spark gap that was used for the trigger voltage pulse switching. This would improve the voltage pulse risetime, as well as the adverse effects of the asymmetrical position of the trigger electrode in the trigatron spark gap for negative hold-off voltages.

The annular rail gap switch is in fact currently employed in the KrF laser facility at the University of

Alberta for a similar application as that described above. It has replaced a master (3-electrode spark gap) switch that triggers all of the 13 spark gaps in the laser. With a load of up to 18-75ohm transmission cables, the rail gap switch provides a reliable voltage pulse at a minimum rate-of-rise of 2.9kV/ns. between 10 and 50kV.

In conclusion, for practical applications of this spark gap design, a sawtooth electrode provides the best switching performance. A +/+ polarity combination is recommended if no preionization is applied, although there will be some sacrifice in the low inductance for low jitter. If preionization is employed, a +/- polarity combination provides optimum jitter as well as inductance. Furthermore, it is highly advisable that the rail gap be well shielded because these high voltage switches radiate a considerable amount of electromagnetic noise.

REFERENCES

1. E.E. Kunhardt, "Electrical Breakdown of Gases: The Prebreakdown Stage", *IEEE Trans. of Plasma Science*, Vol. PS-8, No. 3, pp. 130-138, Sept. 1980.

2. A.A. Offenberger, D.C.D. McKen, R. Fedosejevs "High Power Krypton Fluoride Laser Development For Fusion Energy Research", Final Report to the Energy Resources Research Fund, Contract U-80-14, May 1983.

3. J.R. Murray, J. Goldhar, D. Eimerl, A. Szöke, "Raman Pulse Compression of Excimer Lasers for Application to Laser Fusion", *IEEE J. of Quantum Electron.*, Vol. QE-15, No. 5, pp. 342-368, Oct. 1979.

4. J.M. Meek, J.D. Craggs editors, *Electrical Breakdown of Gases*, John Wiley and Sons, 1978.

5. J.R. Woodworth et. al., "UV-Laser-Triggered Switches", *Proceedings of the Third IEEE Conference on Pulsed Power, Albequerque New Mexico, 1981* pp. 154-156.

6. A.H. Guenther, J.R. Bettis, "The Laser Triggering of High Voltage Switches", *J. Phys. D: Appl. Phys.*, Vol 11, pp. 1577-1611, 1978.

7. Y.H. Tzeng et. al., "The Effect of Electron Beam Induced Space Charge on Spark Gap Breakdown", *Proceedings of the Third IEEE Conference on Pulsed Power, Albequerque New Mexico, 1981*, , pp. 231-237.

8. J.D. Cobine *Gaseous Conductors: Theory and Applications*, pp. 143-196, Dover Publications Inc., 1958.

9. J.J. Thomson, G.P. Thomson, *Conduction of Electricity through Gases, Vol. II: Ionisation by Collision and the Gaseous Discharge*, pp. 470-532, Dover Publications Inc., 1969.

10. E.E. Kunhardt, W.W. Byszewski, "Development of Overvoltage Breakdown at High Gas Pressure", *Physics Review A*, Vol. 21, No. 6, pp2069-2077, June 1980.

11. H. Raether, *Electron Avalanches and Breakdown in Gases*, pp. 124-136, Butterworth and Co. Ltd., 1964.

12. T.R. Burkes et. al., "A Review of High-Power Switch Technology", *IEEE Trans. on Electron Devices*, Vol. ED-26, No. 10, pp1402-1411, Oct. 1979.

13. R.S. Taylor, A.J. Alcock and K.E. Leopold, "Rail-Gap Switches for High Output Energy Excimer Lasers", *Proceedings of the Third IEEE Conference on Pulsed Power, Albequerque New Mexico, 1981*, pp157-160.

VITA

NAME: Lori Lynn Small

PLACE OF BIRTH: Edmonton, Alberta

YEAR OF BIRTH: 1958

POST-SECONDARY EDUCATION AND DEGREES:

University of Alberta
Edmonton, Alberta
1976-1979

University of Toronto
Toronto, Ontario
1979-1980

Degree: B.Sc. in Physics
University of Alberta
Fall, 1980

University of Alberta
Edmonton, Alberta
1980-1983

RELATED WORK EXPERIENCE:

Teacher's Assistant
University of Alberta
1978-1979, 1980-1983

Summer Student
Tri-University Meson Facility
University of British Columbia
Vancouver, British Columbia
Summer, 1979